Downsizing among the lowest mass galaxies

Roberto Terlevich, INAOE
Elena Terlevich, INAOE
Jesus Lopez, INAOE (Master thesis)

IV WORKSHOP "ESTALLIDOS"
Madrid, 26-27 January 2006



Introduction

Dependence of the star formation history on galaxy mass

- How does the evolution depend on the galaxy mass?
- We have known for many years that faint, low mass galaxies on average are bluer than high mass galaxies, and on average have stronger star formation.
- Recently, the interest in this well established observational result has grown, and its implications have been more and more appreciated. In *all* environments, lower mass galaxies have on average a more recent star formation history. This implies that, on average, going to lower redshifts, the maximum luminosity/mass of galaxies with significant star formation activity progressively decreases.
- This "**downsizing effect**" indicates an "**anti-hierachical**" history for the star formation in galaxies, which parallels a similar effect observed for AGNs .

Recent results suggests that the SF takes place in progressively smaller galaxies as time goes on (e.g., Heavens et al. 2004(MOPED collaboration), Bouche & Lowenthal 2005, Juneau et al. 2005, Le Borgne et al. 2005, Shapley et al. 2005).

Bundy, Ellis & Conselice (2005) argue that downsizing also proceeds from early to late Hubble types.

MOPED collaboration results (based in stellar population analysis in local galaxies)

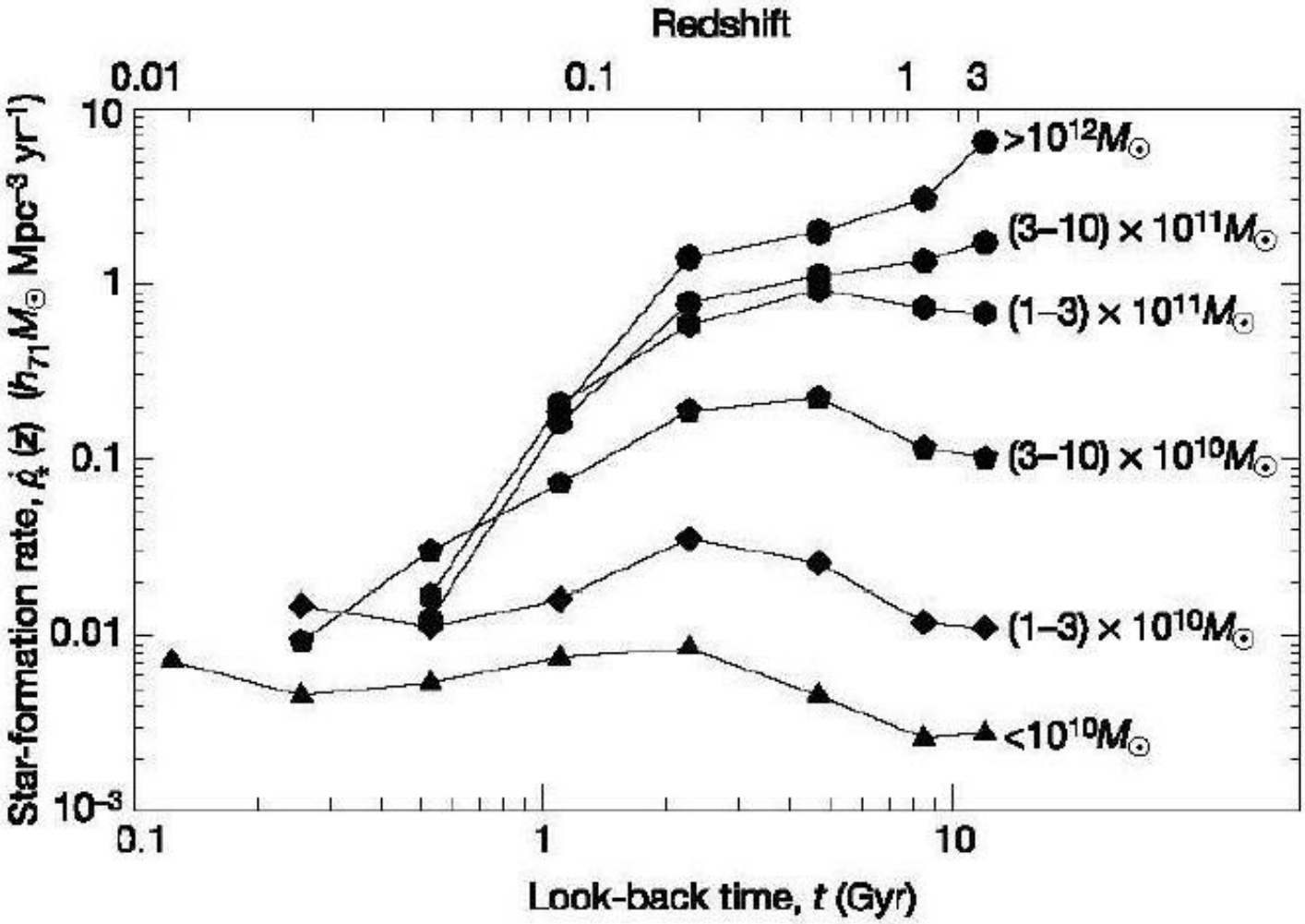
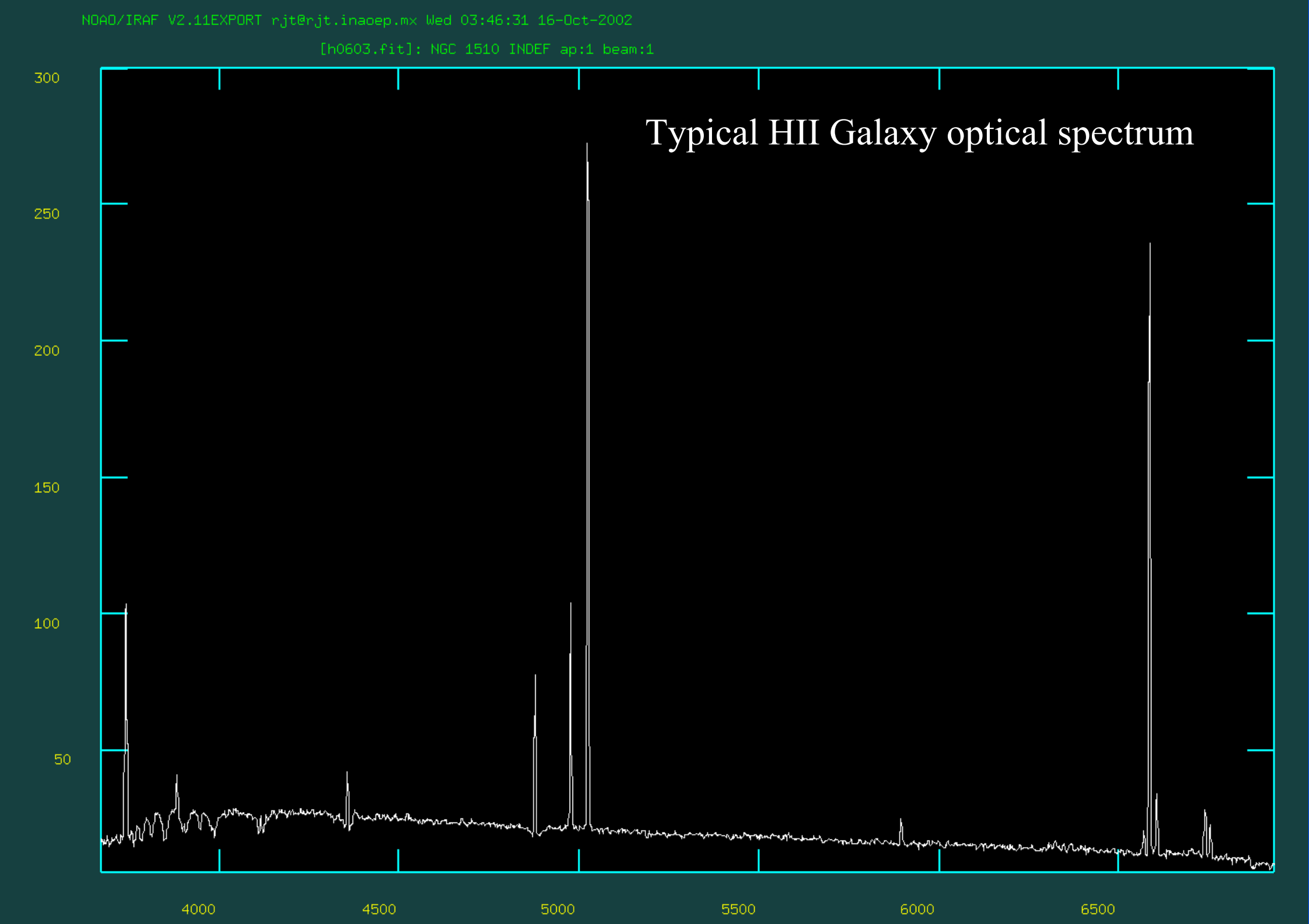


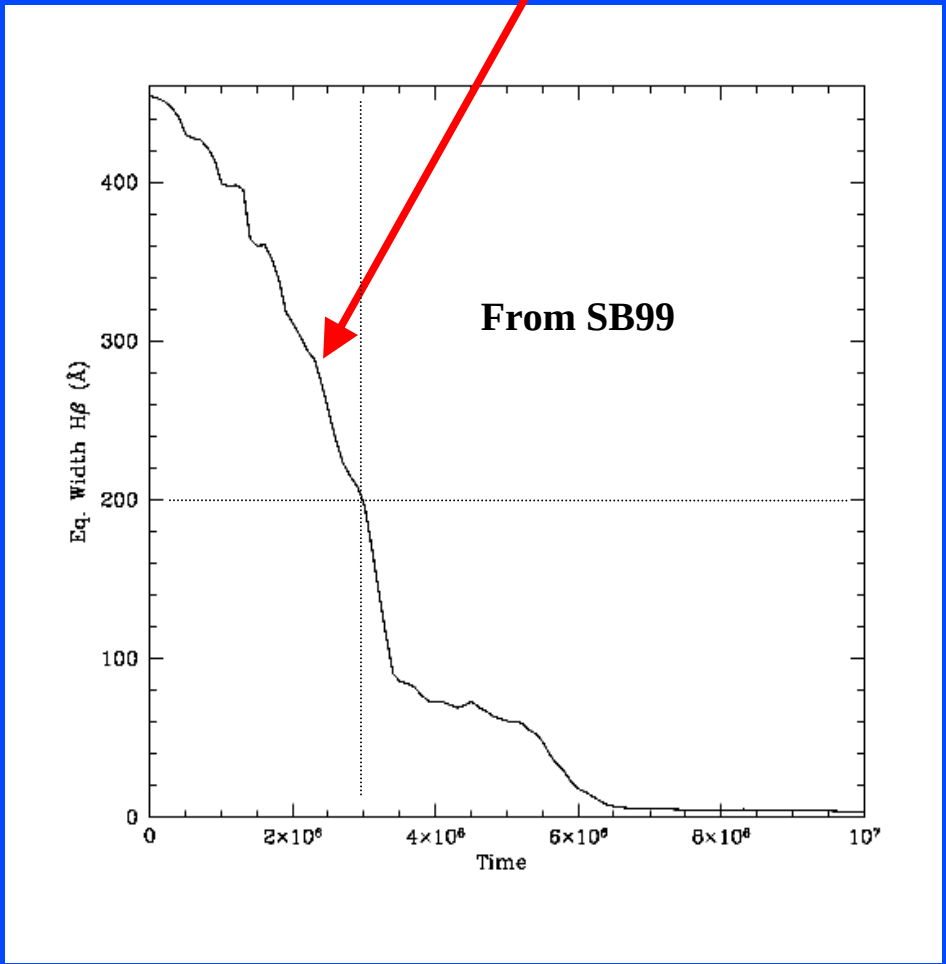
Figure 4.18: SFR vs. lookback time as a function of the galaxy mass (from (Heavens et al., 2004)).

The SF history of HII Galaxies

- Perhaps the youngest i.e. less evolved galaxies are the HII Galaxies.
- HII Galaxies are selected because their optical spectrum resembles that of Superassociations like 30-Doradus in the LMC or NGC 604 in M33.
- HII galaxies tend to be luminous and compact bursts of star formation in low mass galaxies.
- The stellar make-up indicates a young/very young stellar population.
- Their strong emission lines makes them ideal for studies of chemical abundances and chemical evolution.
- Basically, HII galaxies are among the youngest stellar systems that can be studied in any detail.

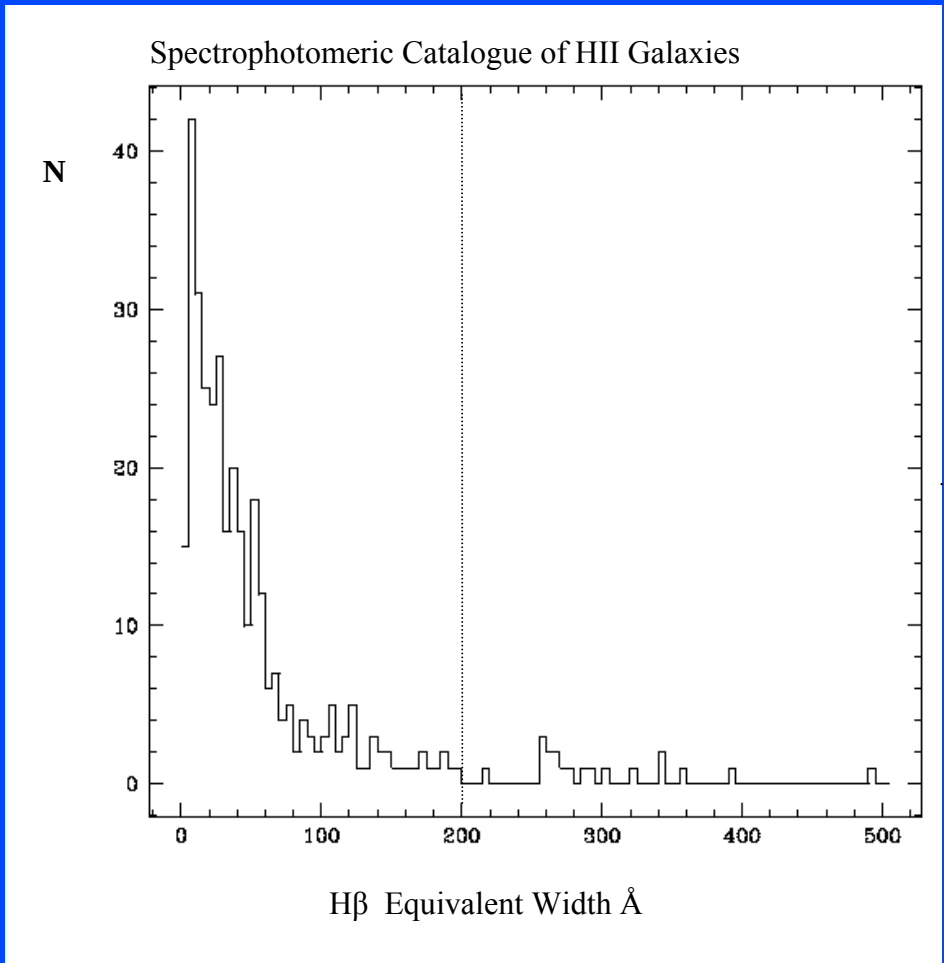

NOAO/IRAF V2.11EXPORT rjt@rjt.inaoep.mx Wed 03:46:31 16-Oct-2002
[h0603.fit]: NGC 1510 INDEF ap:1 beam:1
Typical HII Galaxy optical spectrum
300
250
200
150
100
50
4000
4500
5000
5500
6000
6500

Predicted evolution of the Equivalent width of Hbeta for a coeval burst



If burst are coeval, and given that there is no correlation between bursts between galaxies, catalogues of strong emission line Starburst should show a median Equivalent Width of Hbeta around 200A.

But surveys of strong emission line HII Galaxies find few with EqwHBeta > 200Å



For many years we argued about the possible origin of the apparent lack of strong emission line systems, and the pros and cons of the different explanations without reaching a convincing case.

In collaboration with Daniel Rosa, Sergei Silich and Elena Terlevich we developed a new approach

Terlevich etal 2004

We shown that for a population of **independent events** that have a **monotonic evolution** , the probability density function is:

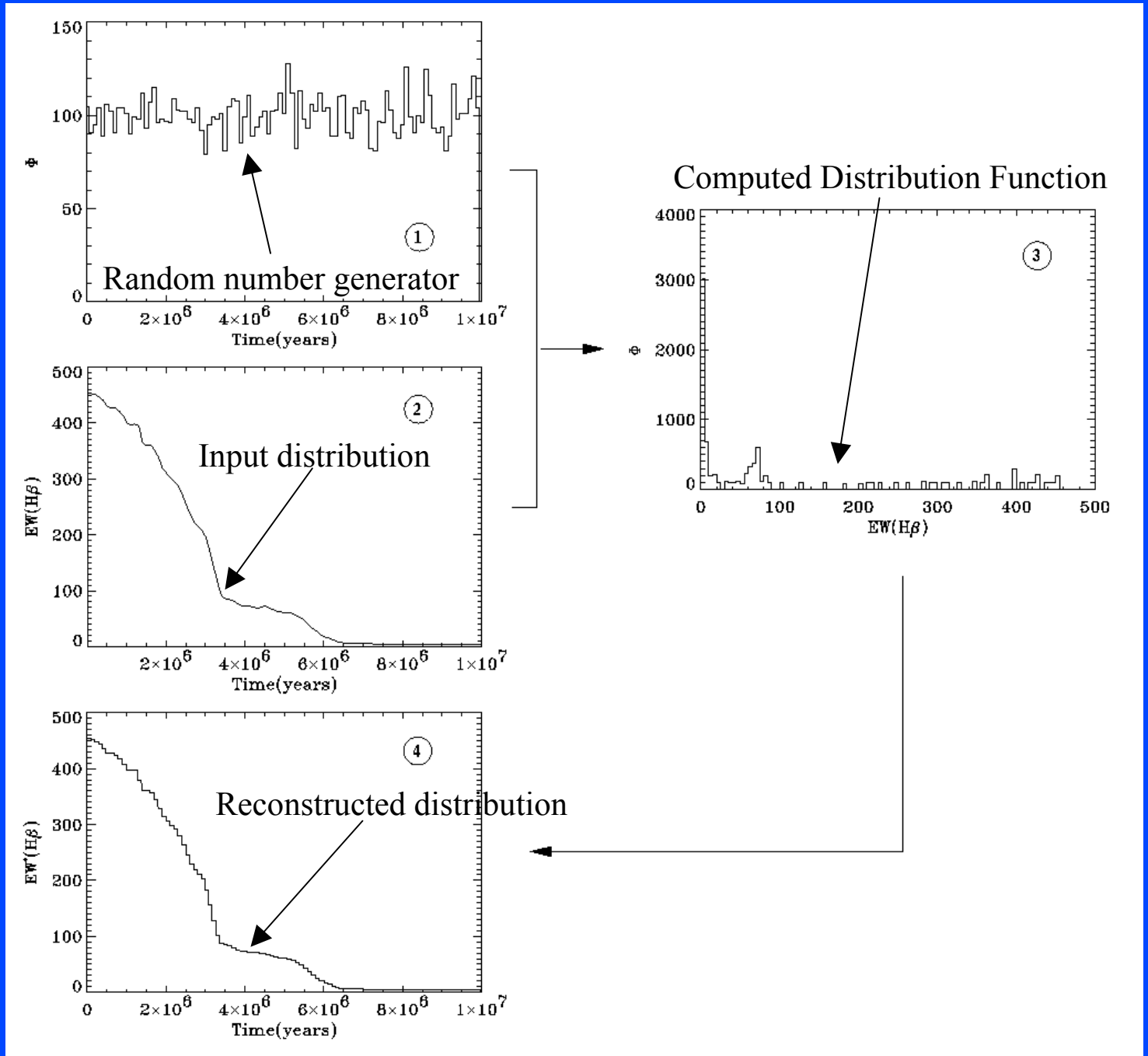
$$\rho_w(W) = -\frac{1}{t_{SF}} \frac{\mathrm{d}t(W)}{\mathrm{d}W}$$

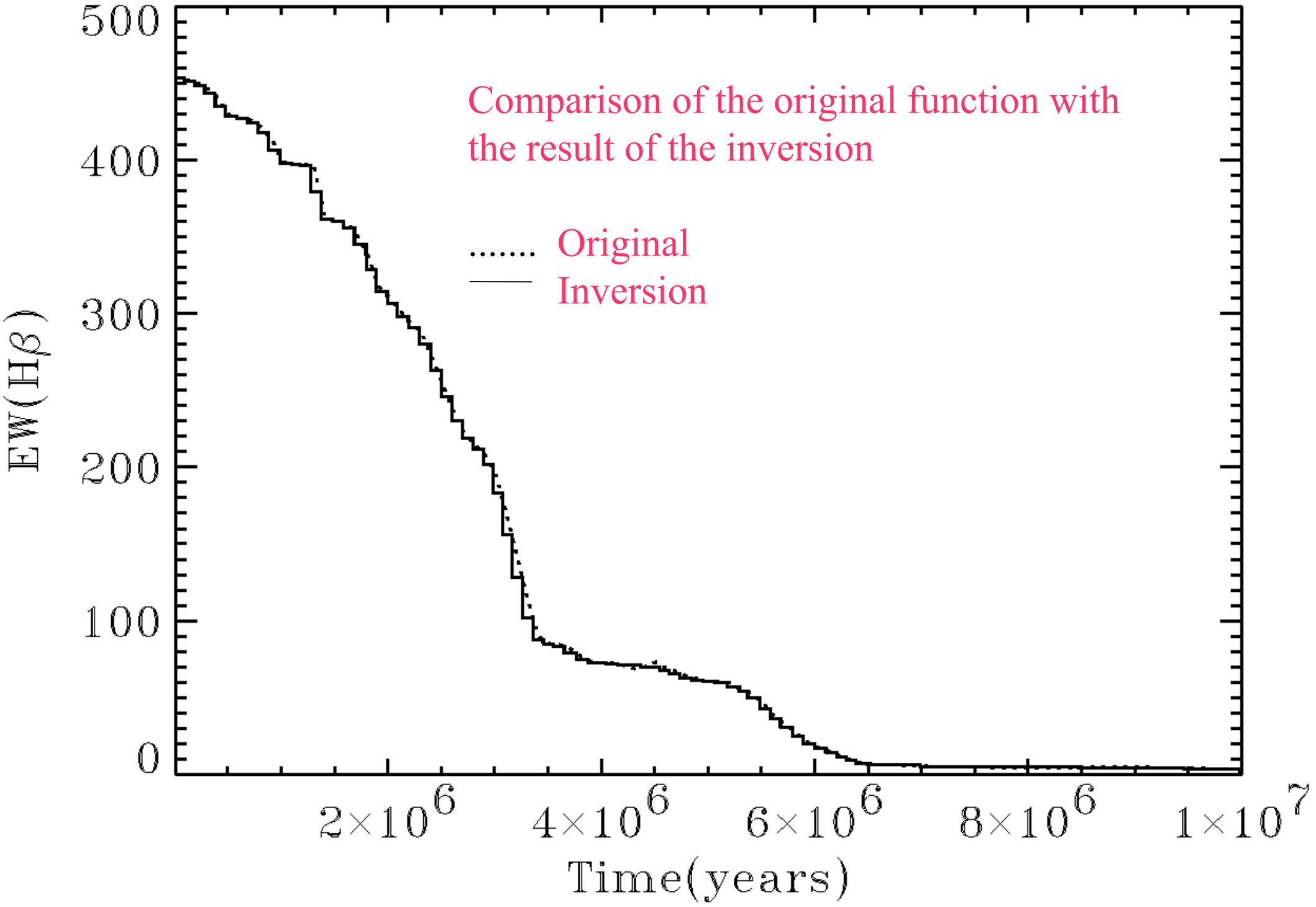
With inverse transformation:

$$t(W) = -\sum_{i_{max}}^{i} t_{SF}\, \rho_i(W)\, \Delta W = \frac{t_{SF}}{N_0} \sum_{i}^{i_{max}} \Delta N_i$$

i.e. the original distribution can be recovered

The Equivalent width evolution case




Comparison of the original function with the result of the inversion
..... Original
—— Inversion
EW(Hβ)
500
400
300
200
100
0
2×10^6
4×10^6
6×10^6
8×10^6
1×10^7
Time(years)

For samples of events that are randomly distributed in time, for parameters that evolve monotonically, it is possible to recover the shape of its time dependence .

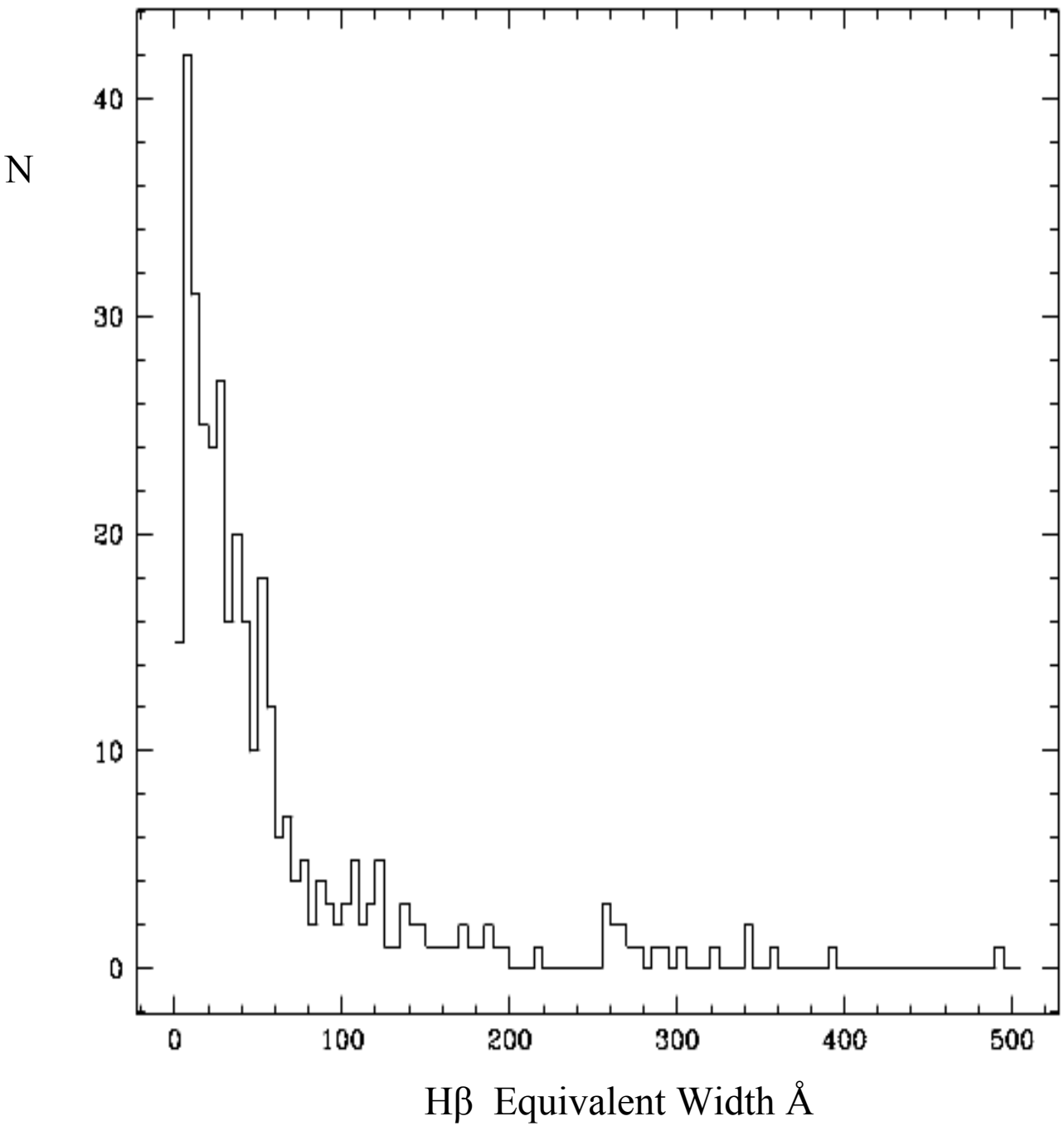
The reconstructed distribution has an undetermined scale factor.

Initially we applied the inversion method to 3 different samples:

1 – SCHIIG that includes the youngest systems

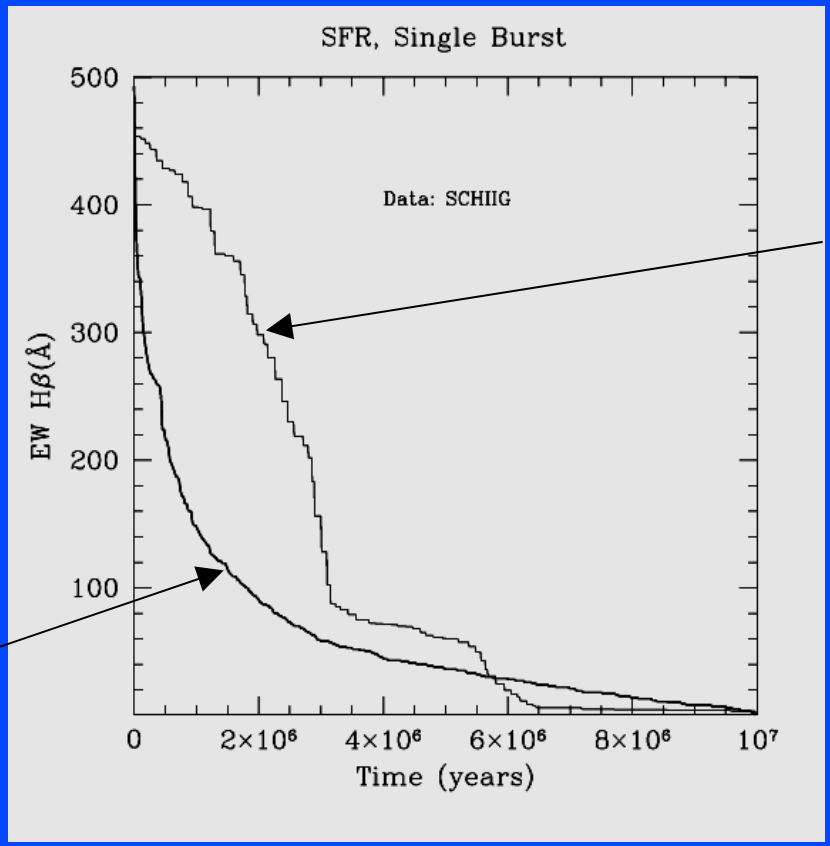
2 – UCM complete sample of nearby emission line galaxies

3 – Sally Oey's sample of HII regions in spirals



Observed distribution from the Spectrophotometric Catalogue of HII Galaxies.

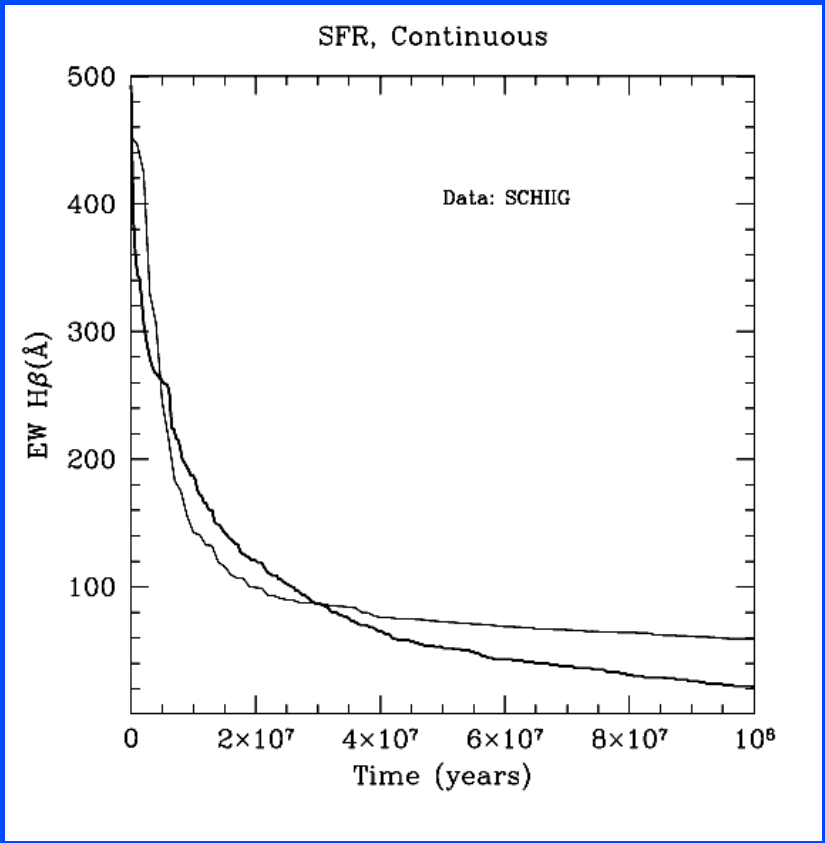
Instantaneous SF (SCHIIG)



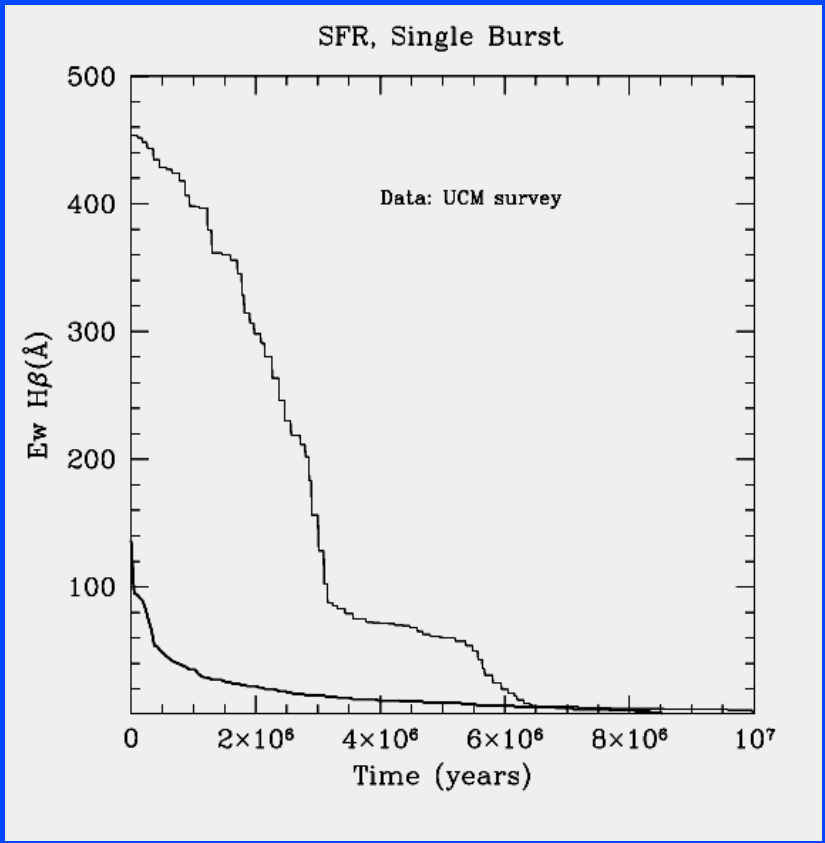
Model prediction

Inversion from data

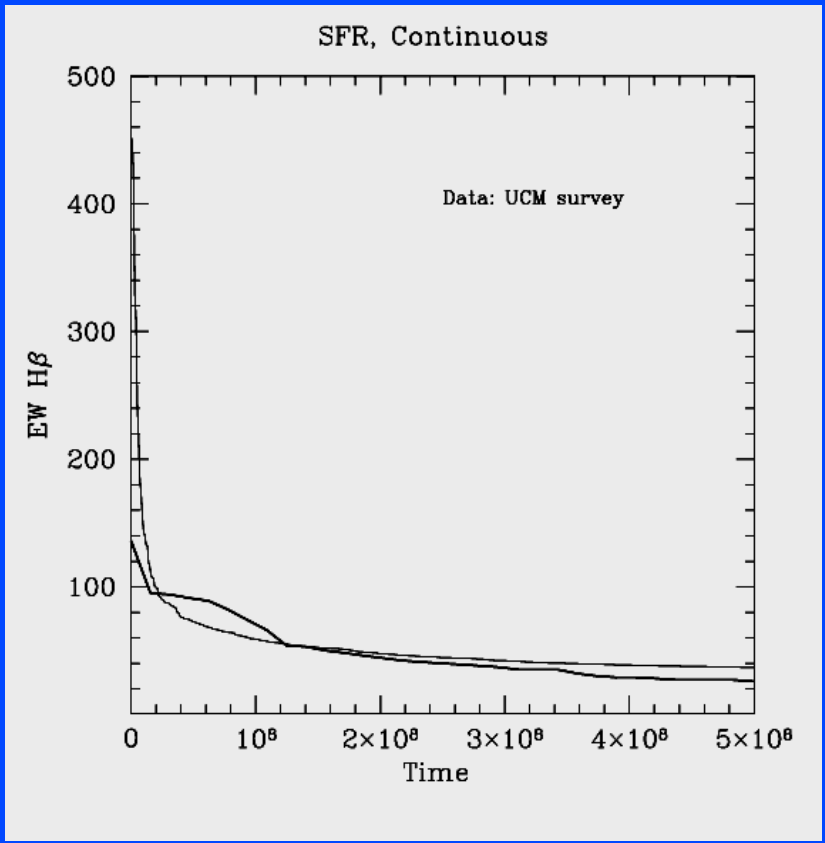
Continuous SF (SCHIIG)



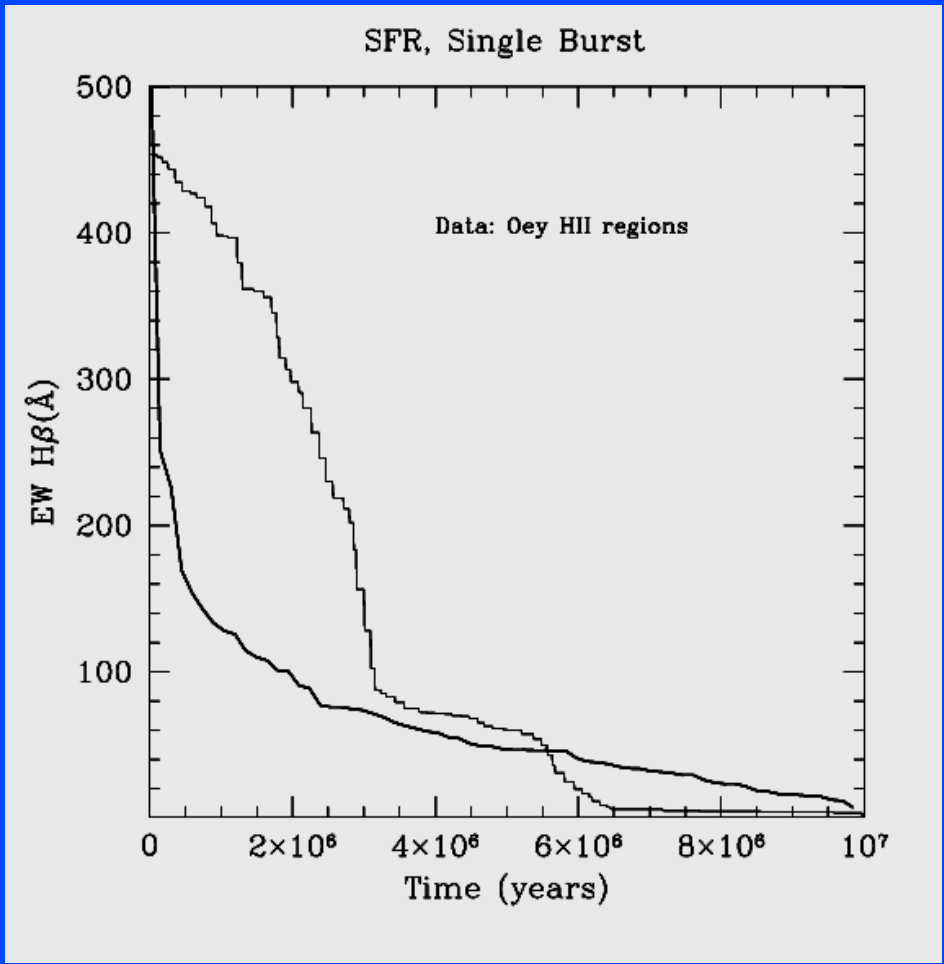
Instantaneous SF (UCM)



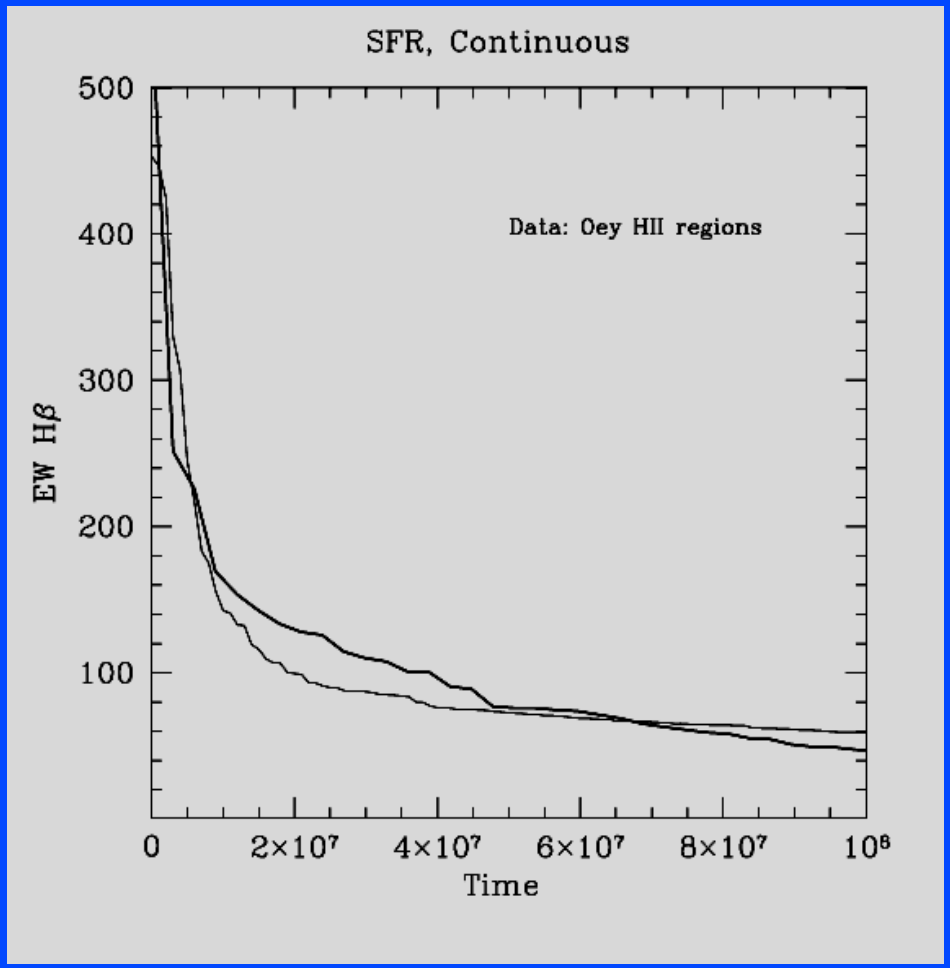
Continuous SF (UCM)



Instantaneous SF (Oey's HII regions)



Continuous SF (Oey's HII regions)



Results are similar for the SCHIIGx and UCM sample and also in individual HII regions in spiral arms.

Single Burst model predictions do not fit the shape of the observed evolution of the Equivalent width of Hβ.

Continuos SFR models give a reasonably good description of the shape of the evolution of the Equivalent width of Hβ.

The conclusion is perhaps obvious:

While the observed emission lines in HII galaxies track the present burst properties, the underlying continuum contains the whole history of SF.

Application to SDSS HII galaxies

- The availability of large number of good spectra of HII galaxies from SDSS prompted us to investigate the history of SF in HII galaxies for a range of masses and metallicities
- Of the more than 500,000 emission line galaxies of SDSS DR3 we selected those with the strongest Halpha emission line (EWHa>100A)

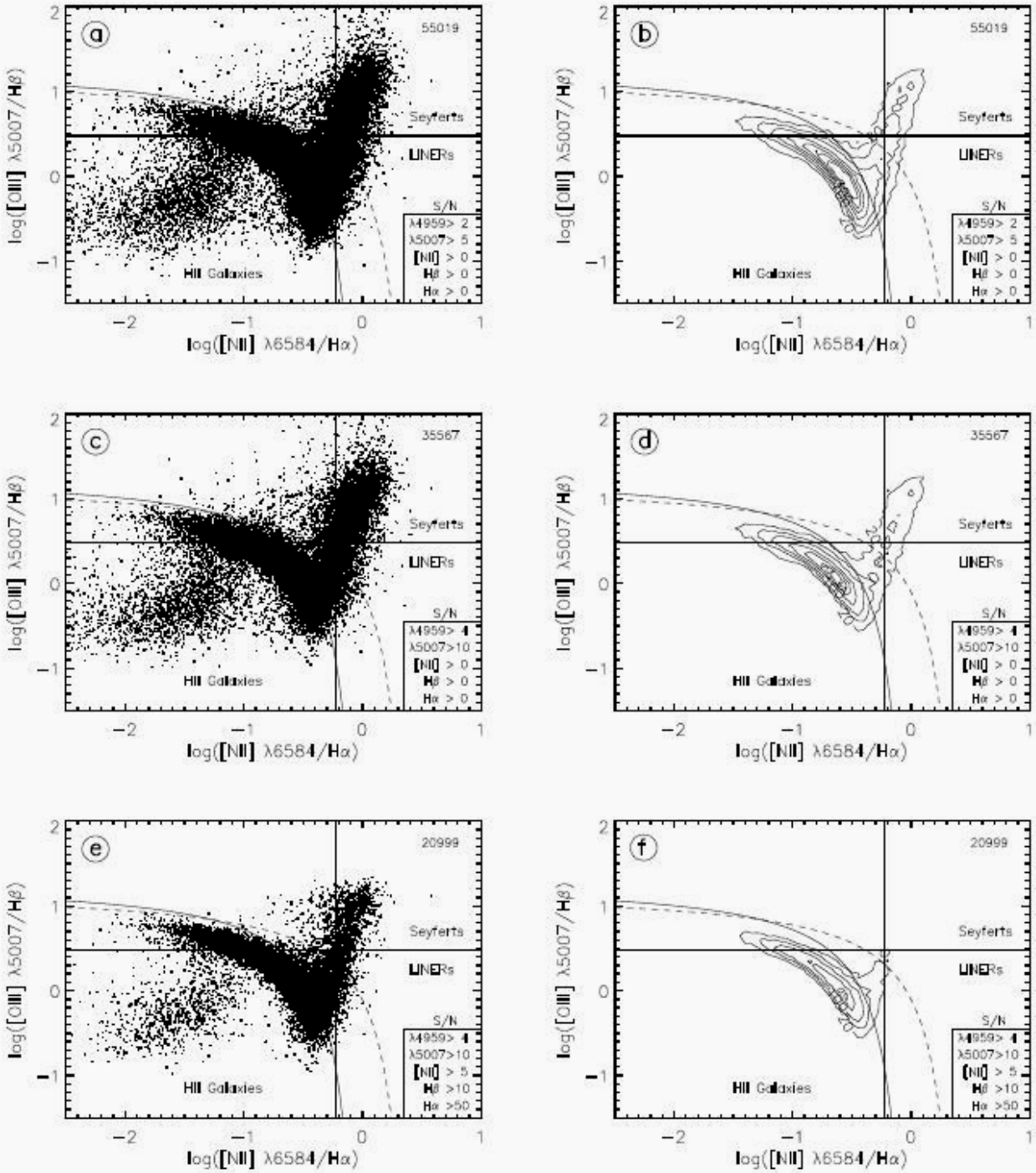


Figure 2.9: Diagnostic diagrams with increasing S/N restrictions. Each panel shows in the upper right corner the number of objects in the plot and in the lower right the S/N conditions.

BPT diagram showing the effect of constraining the S/N of the data

Excluded objects

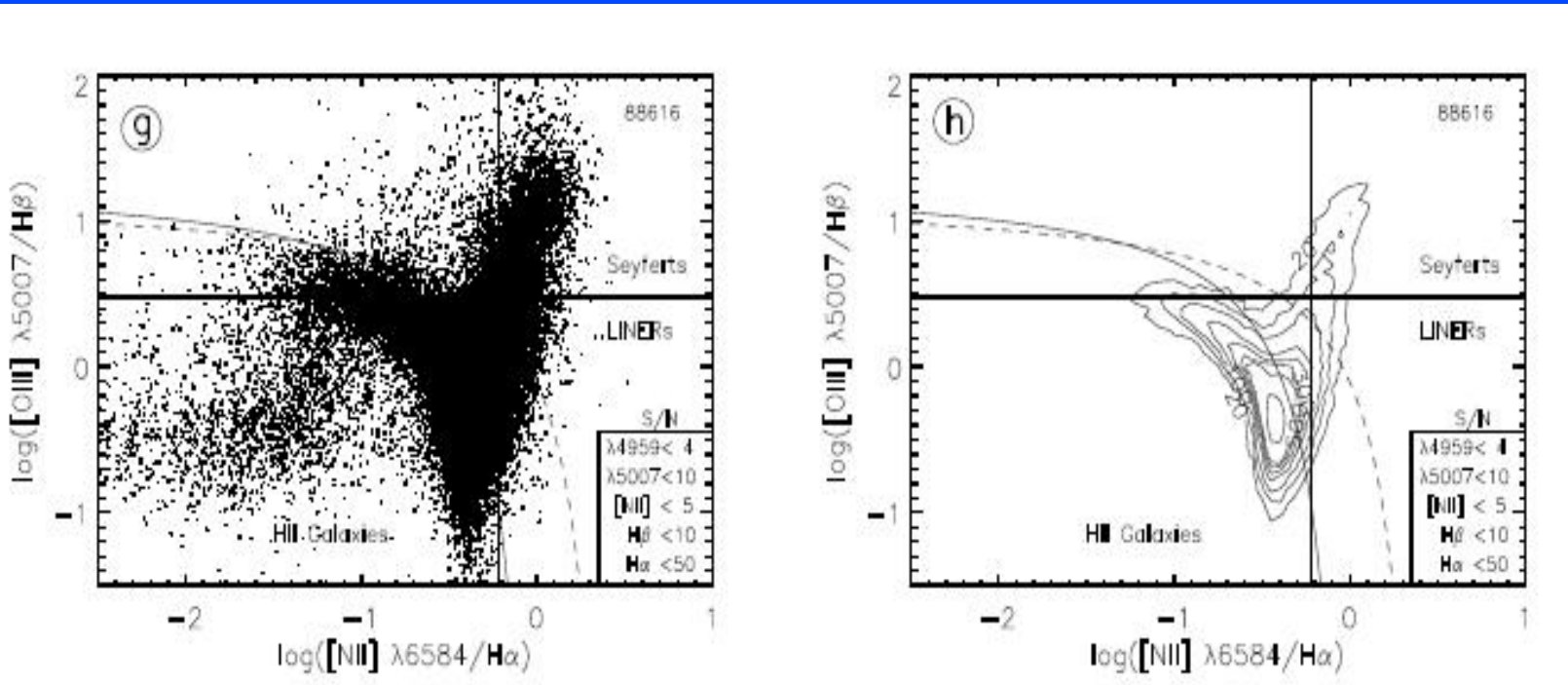


Figure 2.10: Diagnostic diagrams for the excluded objects

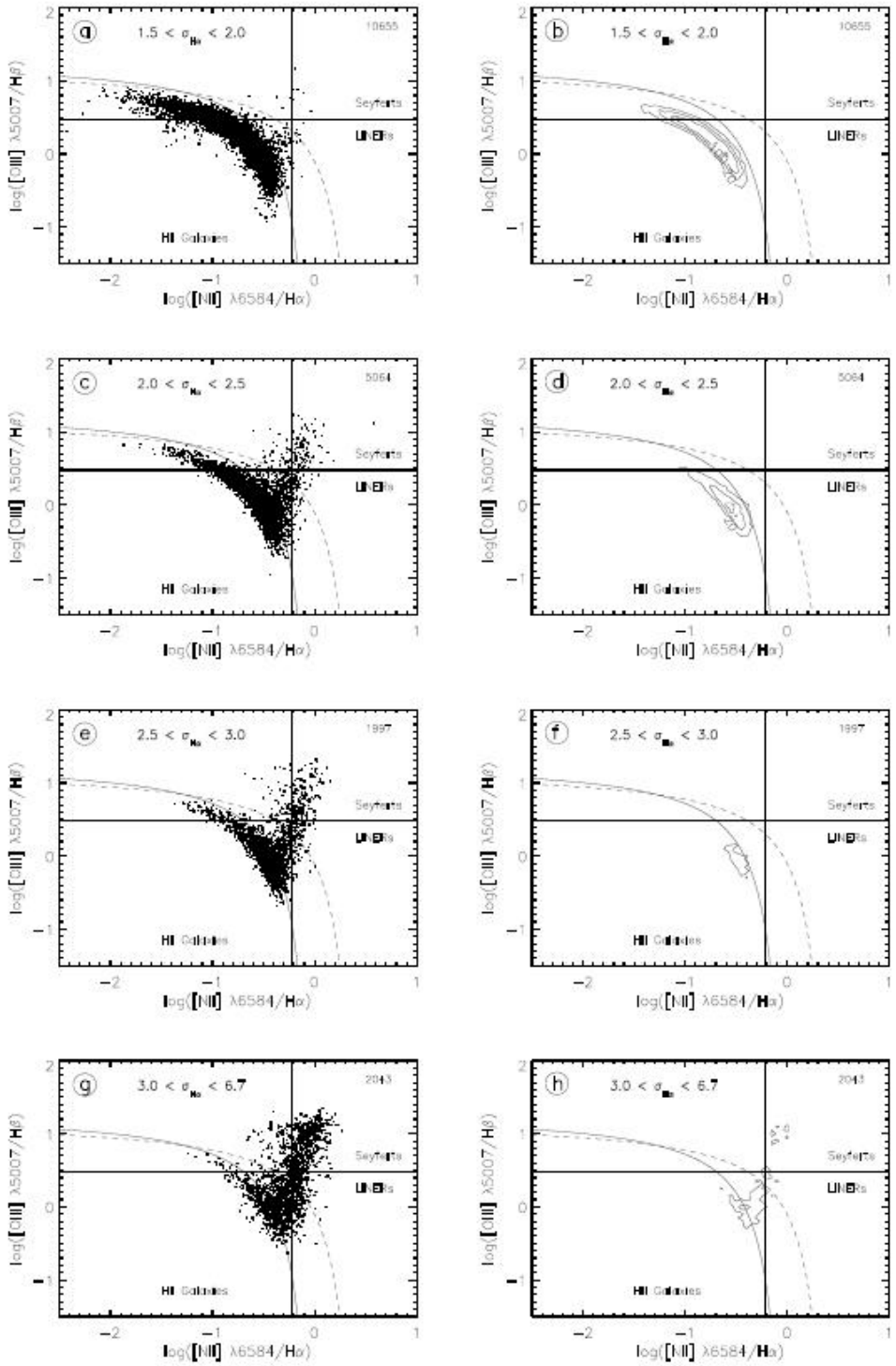


Figure 2.12: Use of $\sigma_{\mathrm{H}\alpha}$ as an extra parameter to reject Seyfert galaxies and LINERs

Population of the BPT diagram for different emission line widths

Objects outside the line width limits.

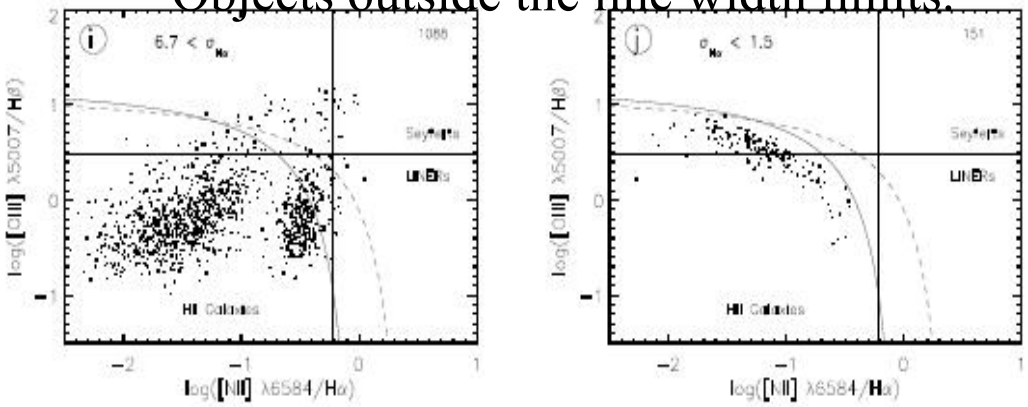


Figure 2.13: Objects below and above the $\sigma_{H\alpha}$ limits in figure 2.12

Final sample

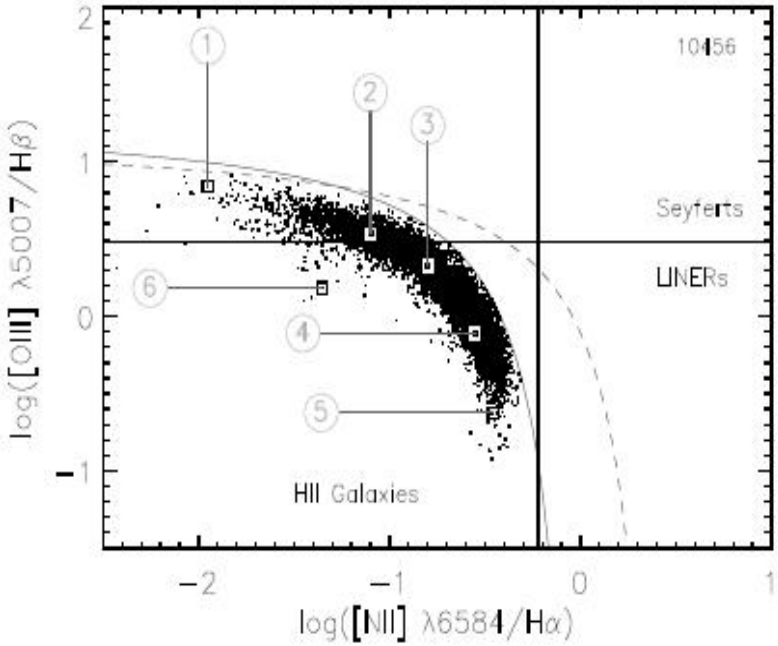


Figure 2.14: BPT diagram for the final sample. Squares indicate selected objects to show their spectra in plot 2.16.

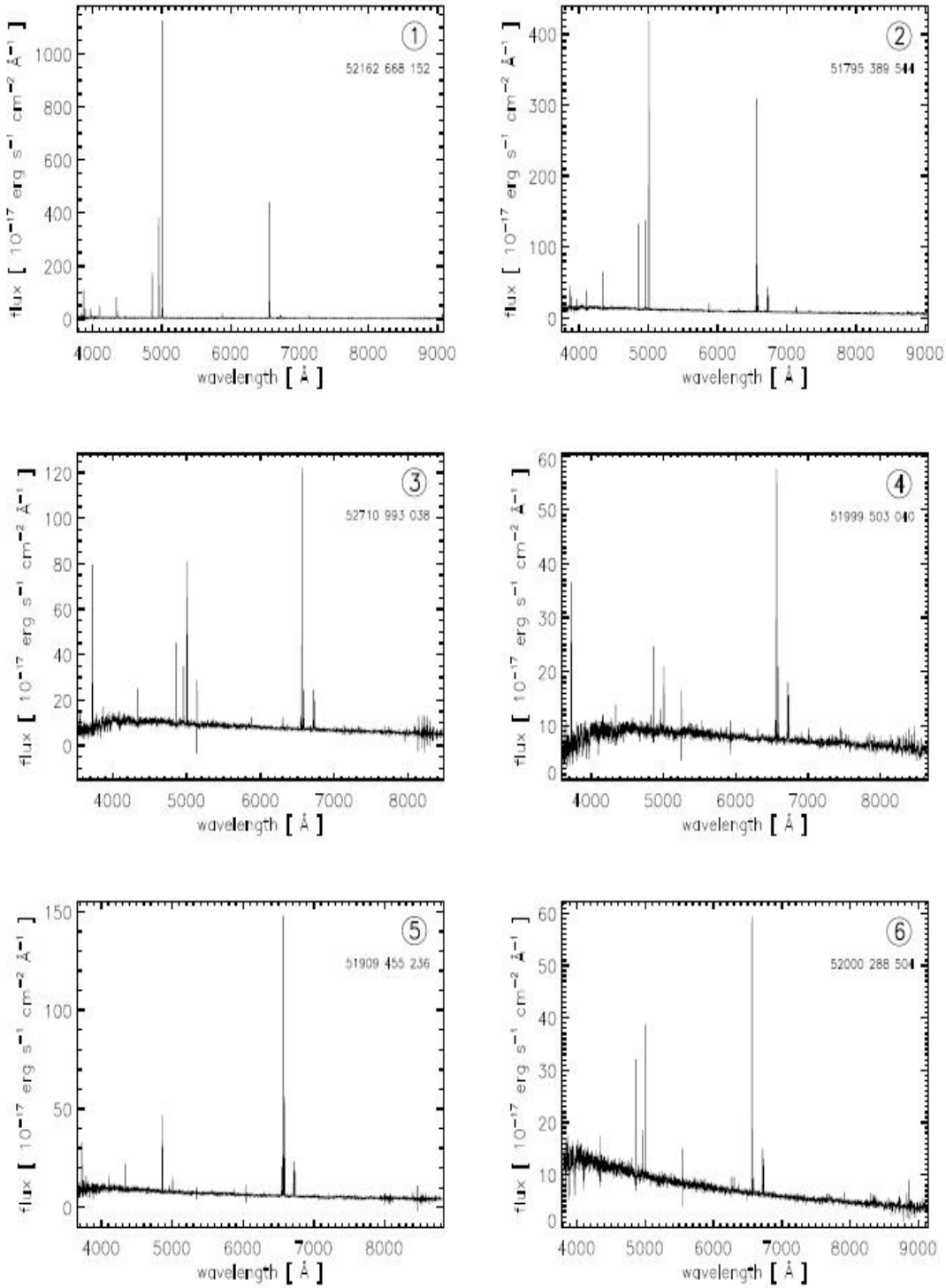


Figure 2.16: Spectra for the selected objects in figure 2.14.

Final sample isocontours

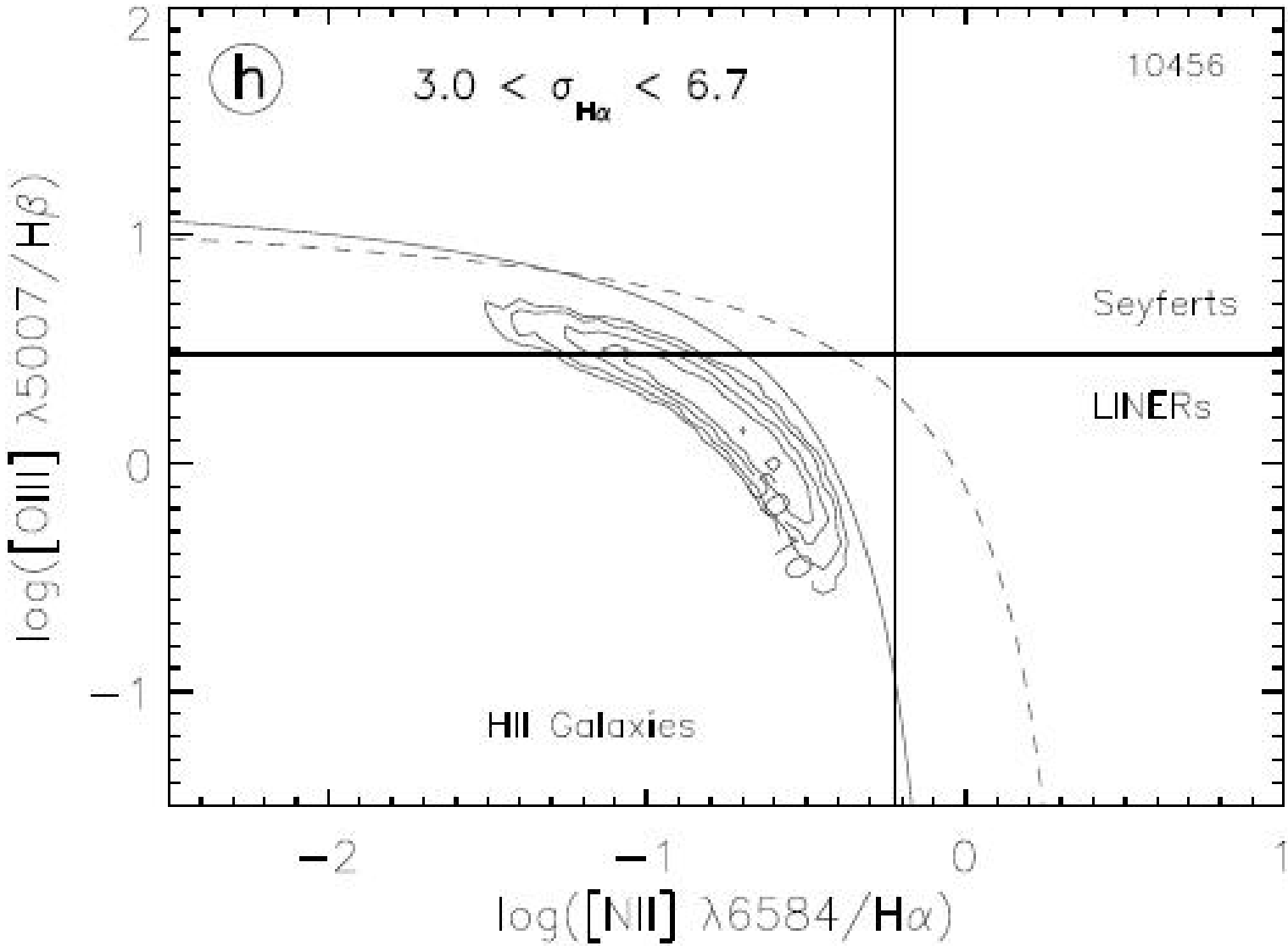


Figure 2.15: Isocontours for the BPT diagram for the final sample.

Halpha EW distribution

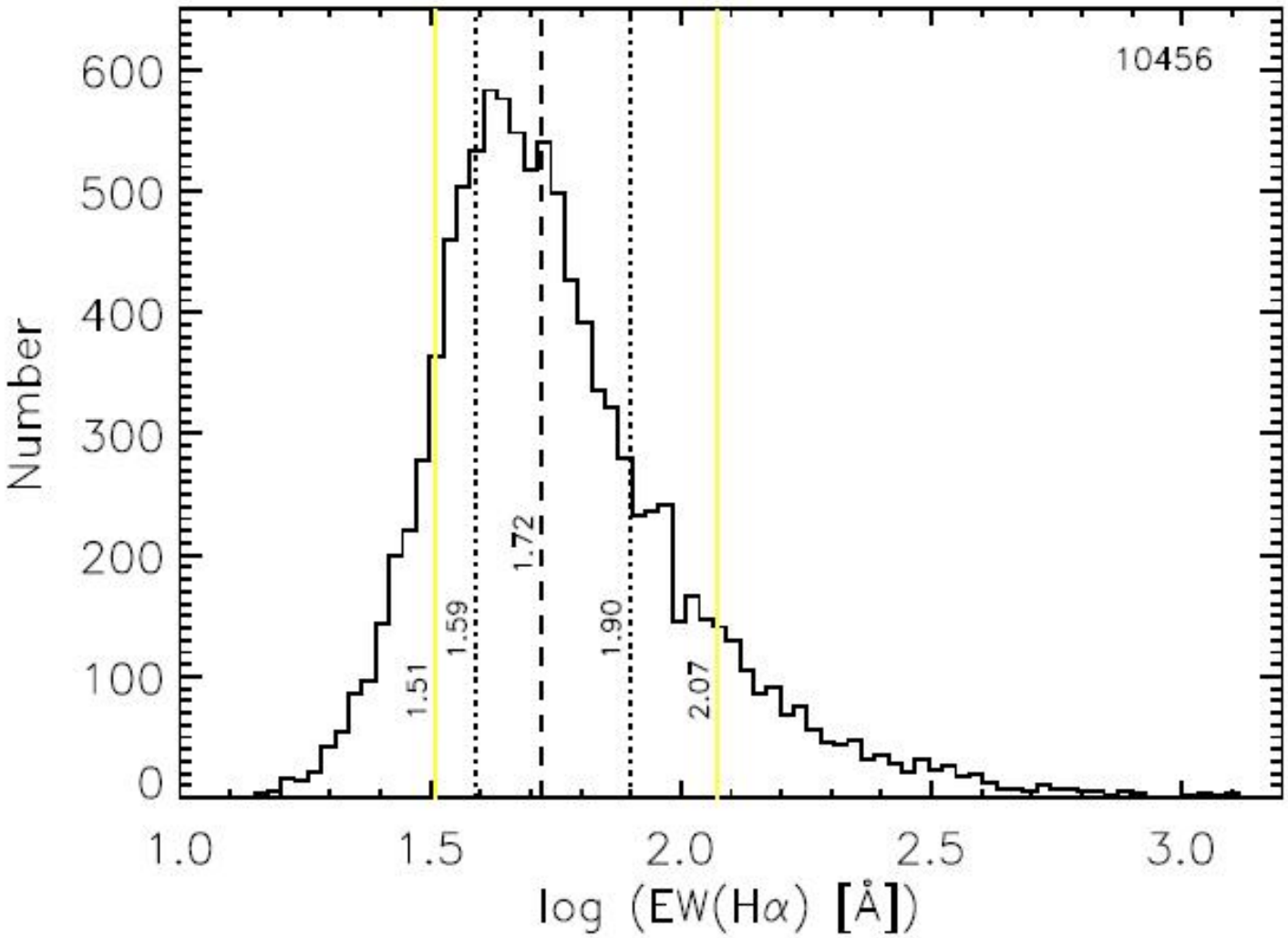


Figure 3.1: Distribution of EW(Hα). The dashed line indicates the median, dotted lines are for 25% and 75% of the distribution and grey lines are for 12.5% and 87.5% (first and last octiles).

Halpha EW vs time

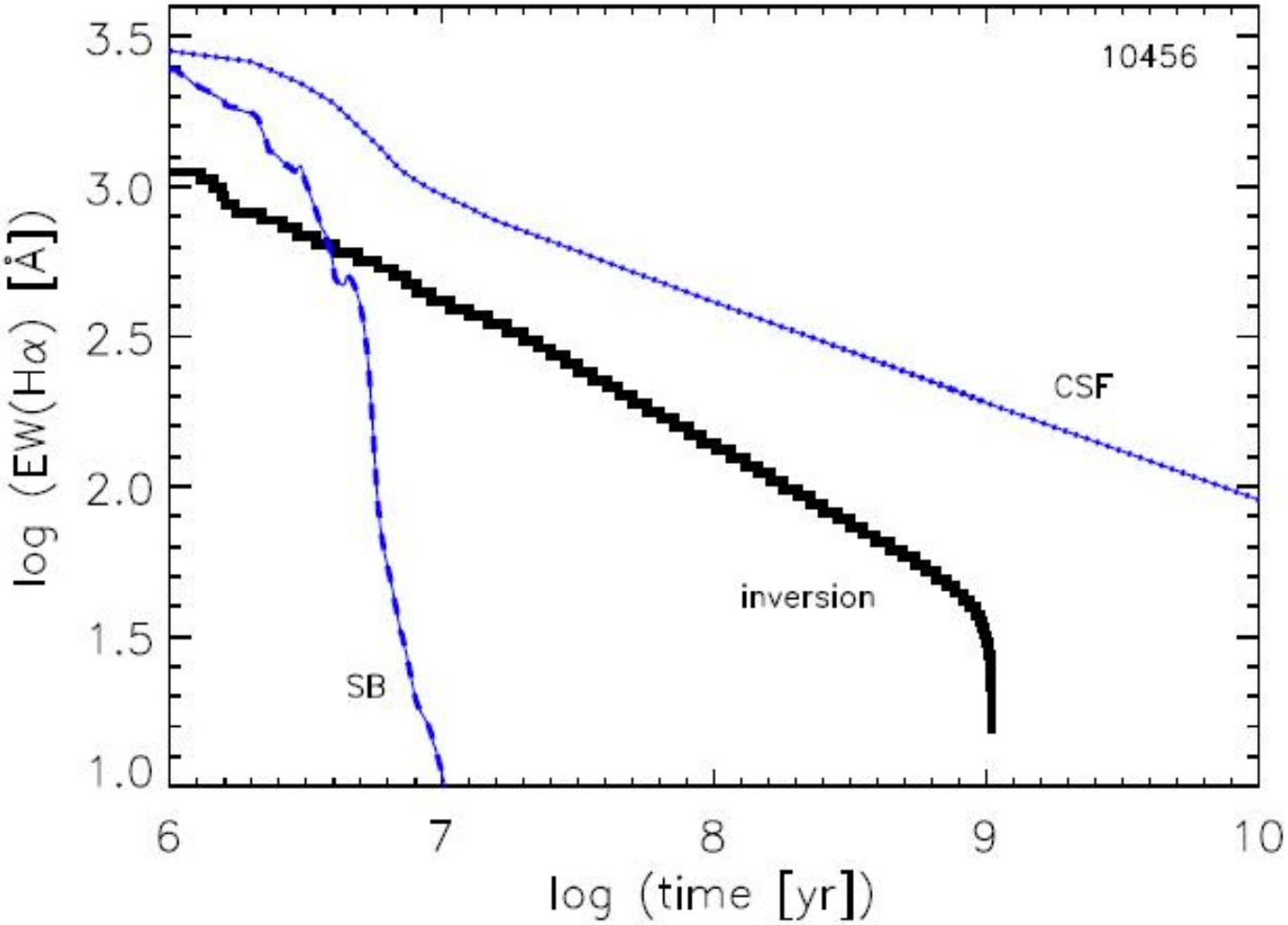


Figure 3.3: Recovered EW(Hα) distribution vs. log (time [yr]), obtained from the inversion procedure: corrected by underlying absorption (solid black line) and uncorrected (gray solid line). SB99 simulations results are included: CSF (dotted line) with $1 M_{\odot}$ yr^{-1} and SB (dashed line) with total mass equal to $10^6 M_{\odot}$.

Optical continuum luminosity distribution

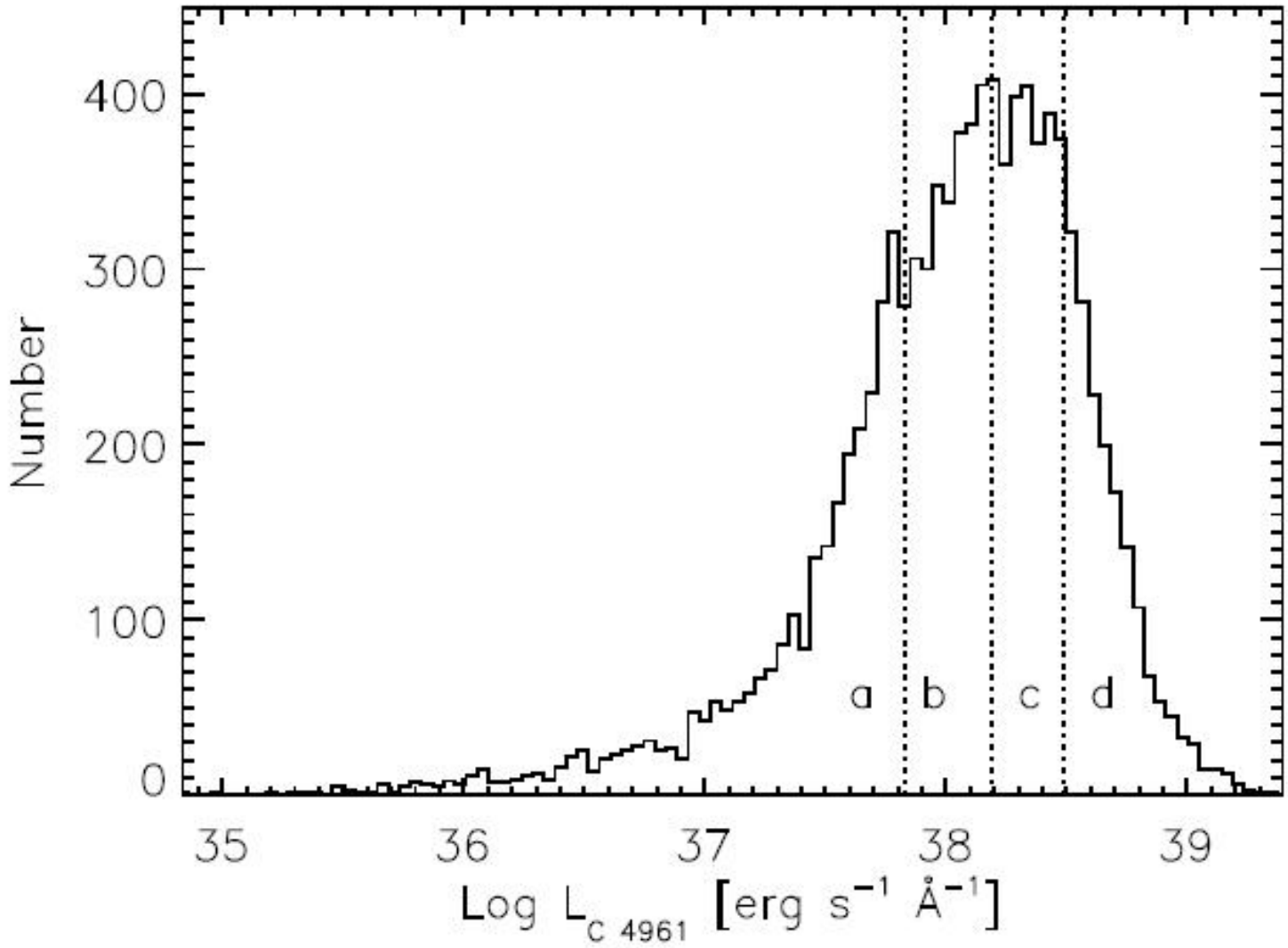


Figure 3.6: Log L_{C4861} distribution for the sample. The dotted lines indicate the limits that divide the sample in quartiles.

Optical continuum luminosity dependence

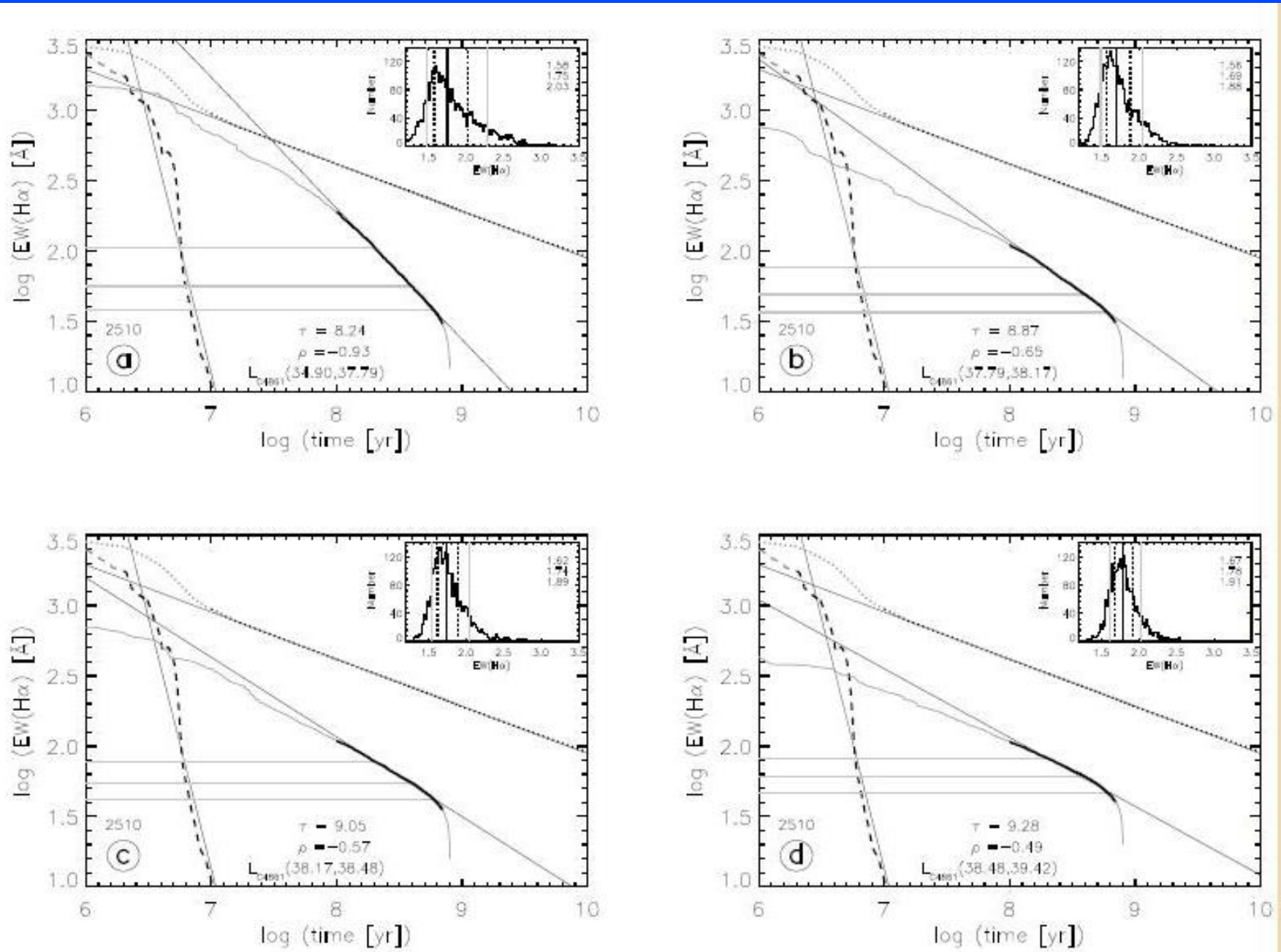


Figure 3.7: Inversion for the different subsamples with increasing L_{C4861}, letters correspond to the bins indicated in figure 3.6. The number of objects is above the letter. The insert in the upper right corner of each panel shows the EW(Hα) distribution used for the inversion.

Models with decreasing SFR

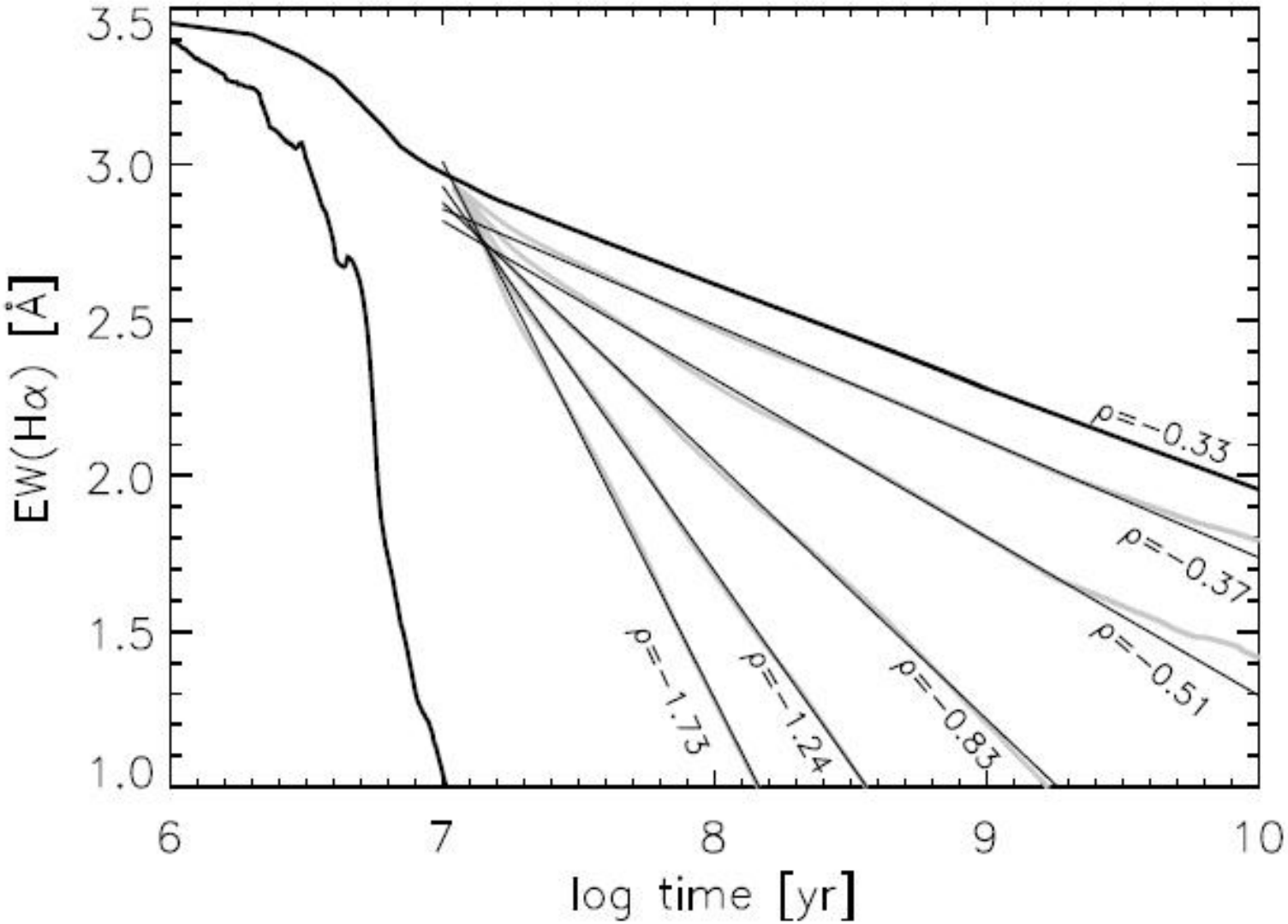


Figure 3.4: Models (kindly calculated by S. Silich) with decreasing star formation power law. The lines are for $SFR \propto t^{\mu}$ where μ is 0.0, -0.5, -1.0, -1.5, -2.0 and -2.5 starting from the CSF mode. ρ is the slope for each line.

Ajustes

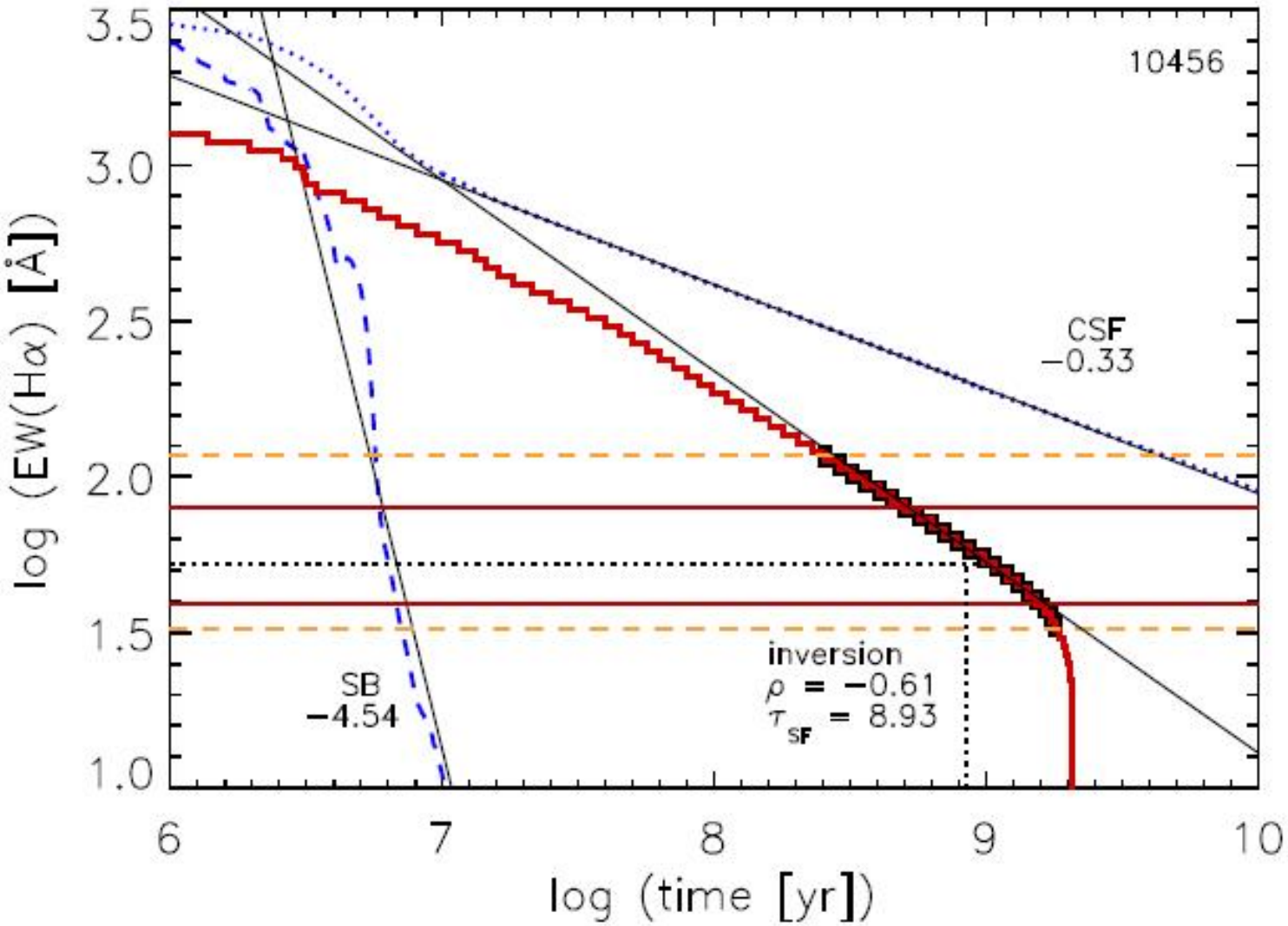


Figure 3.5: Log EW(Hα) vs log time. It shows the use of slopes to allocate time in the inversion from figure 3.3. The solid lines are approximations to the models and the inversion (excluding the first and last octiles), the number below each label is the associated slope. The timescale obtained is $\tau_{SF} = 8.93$

Optical continuum Luminosity vs AGE

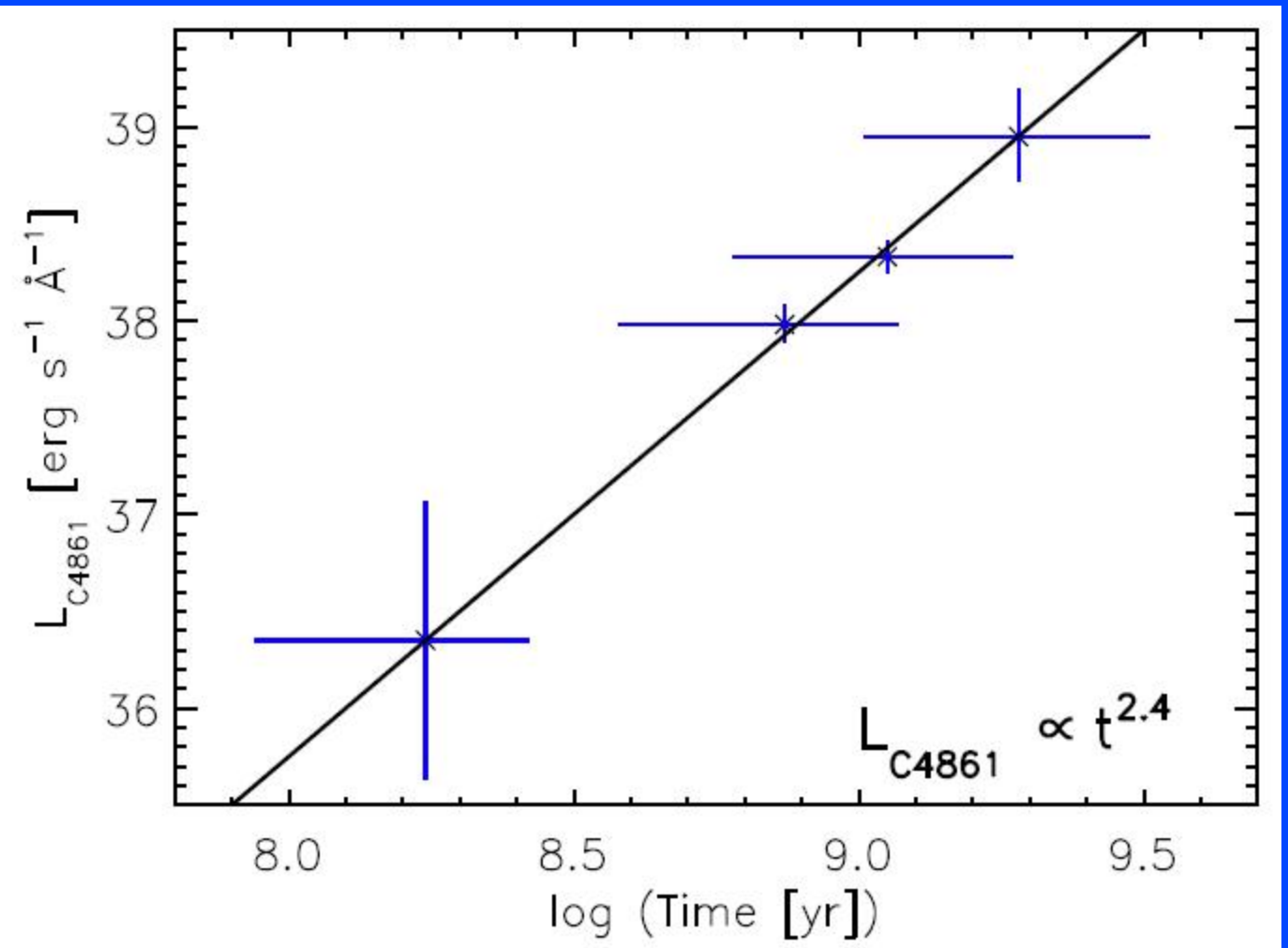


Figure 3.8: L_{C4861} vs Time.

More luminous galaxies (starlight) are older

Metallicity distribution

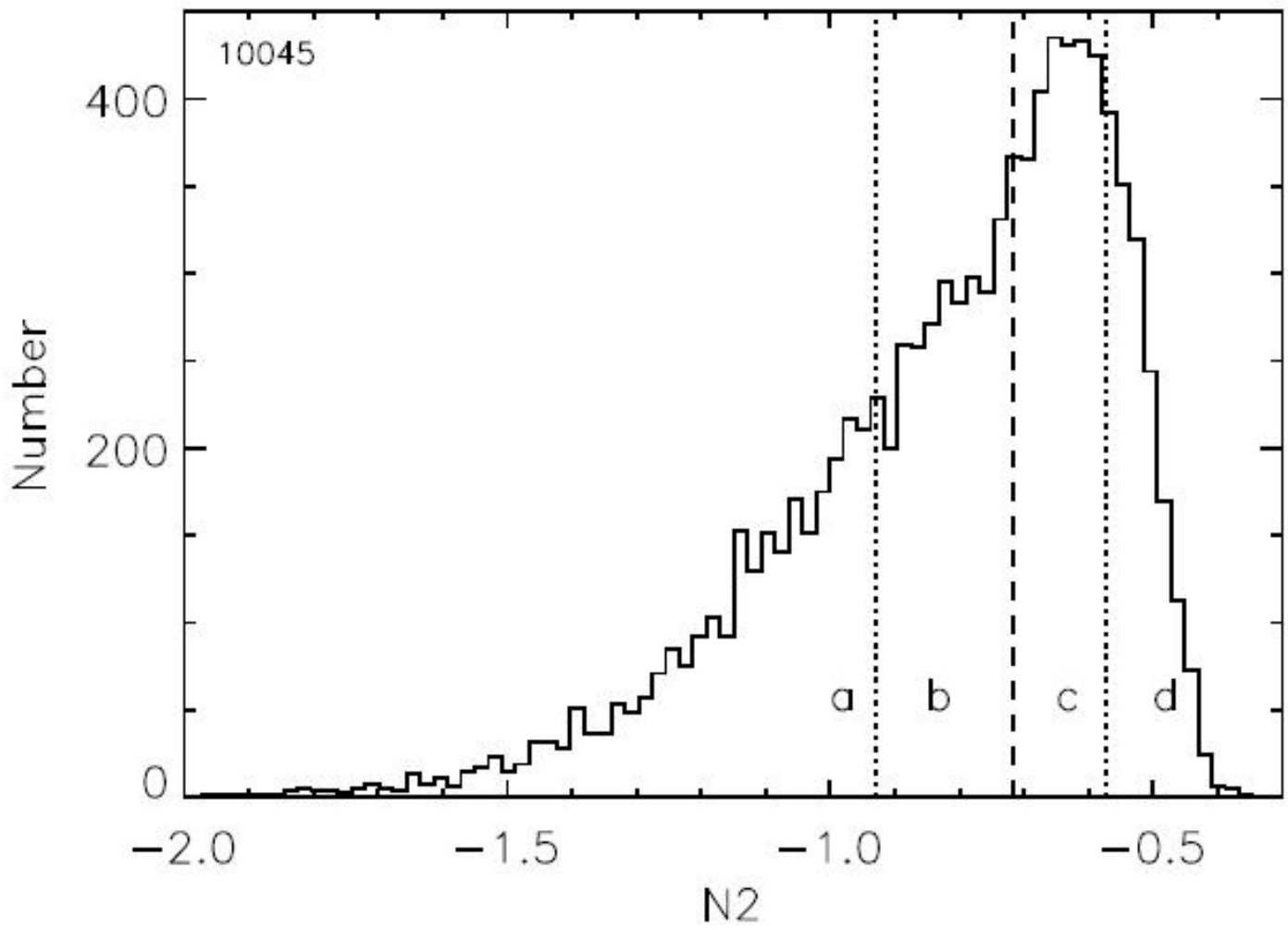


Figure 3.14: Distribution of galaxies from the sample over metallicity. N2 is used as indicator of the average ISM metallicity. Dashed line indicate the median and dotted lines the 25% and 75% of the distribution

Metallicity dependence

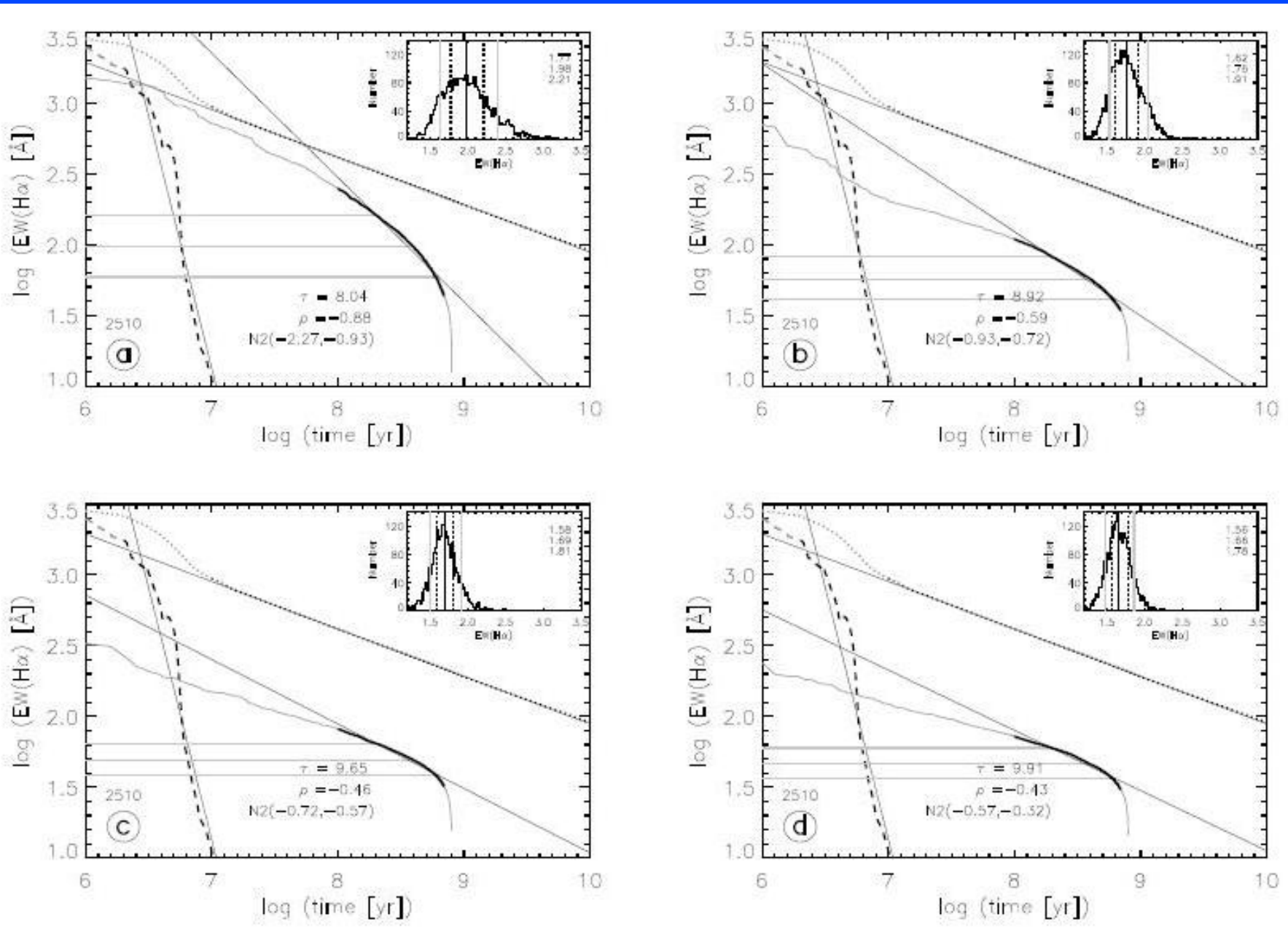


Figure 3.15: Inversion for data subsets of increasing metallicity (N2). The letters correspond to the bins in figure 3.14

Extremely low metallicity range

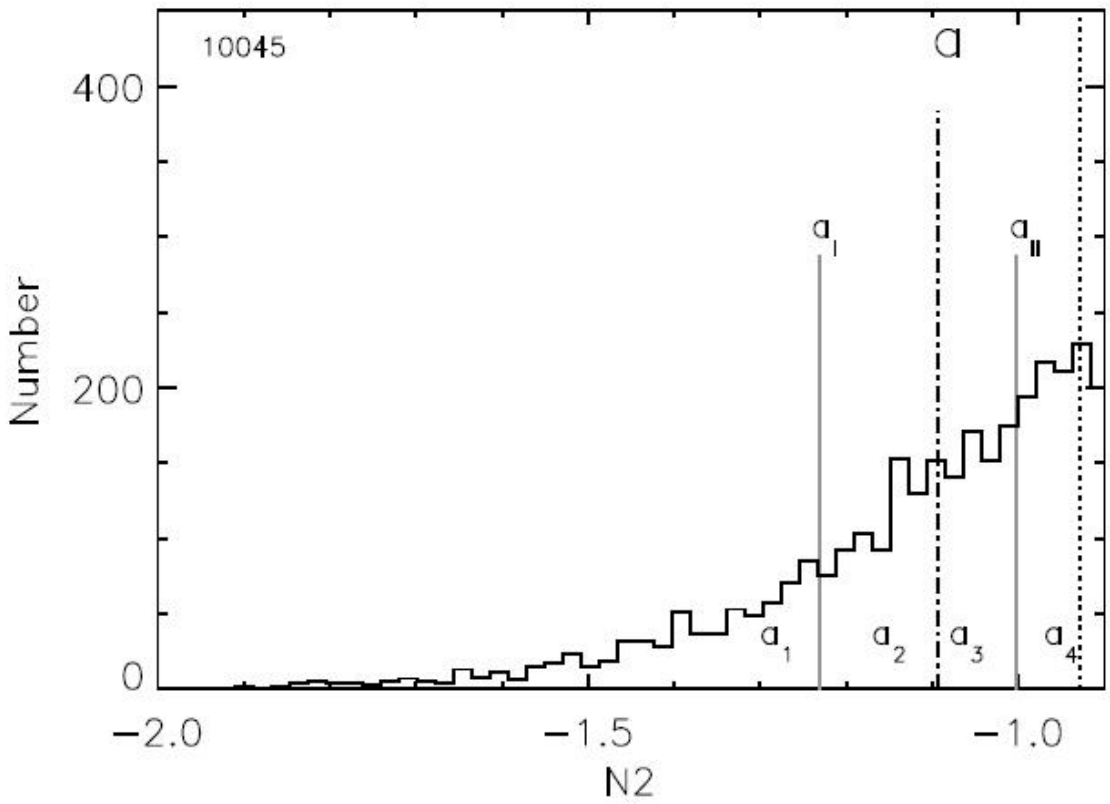
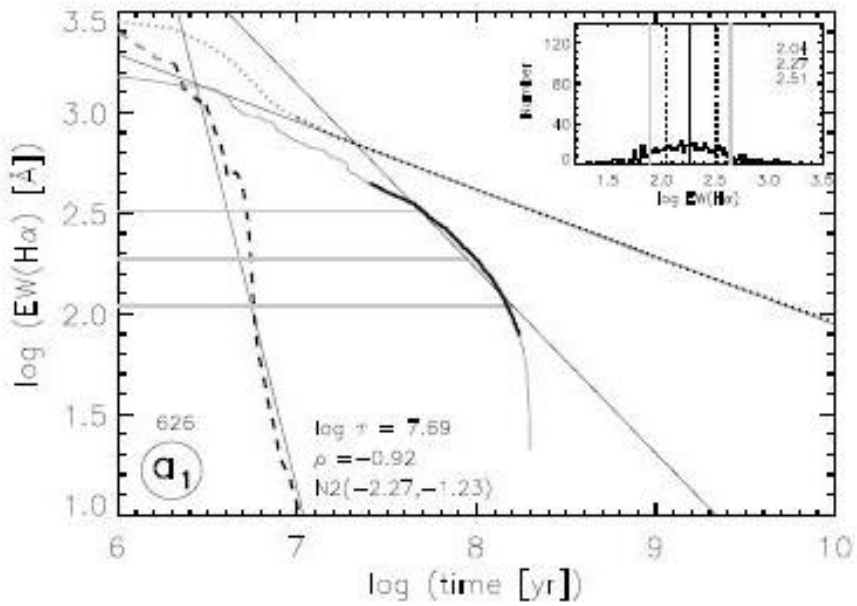
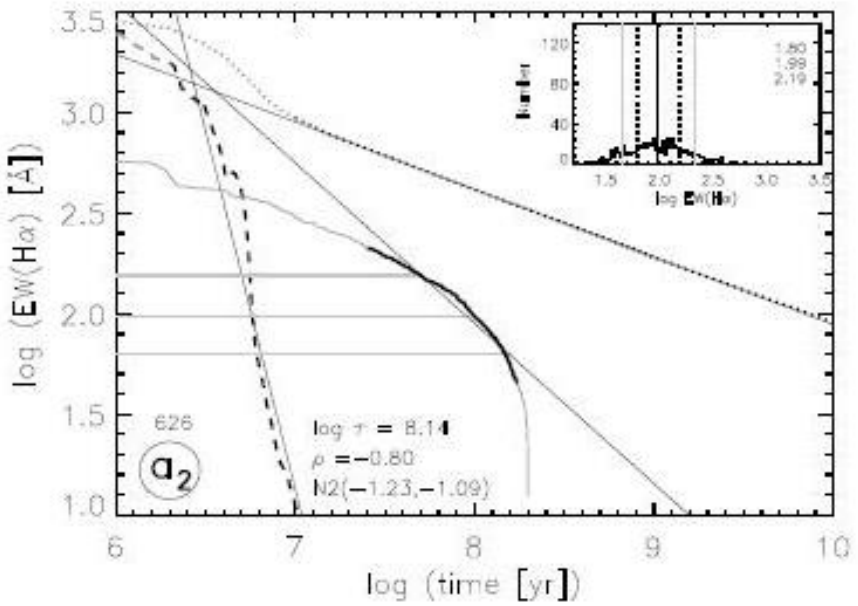
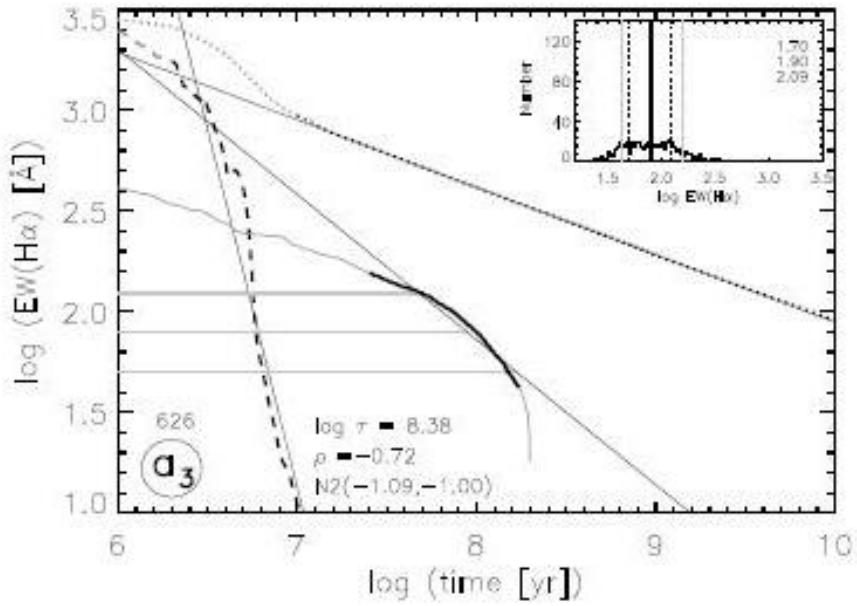


Figure 3.16: The lowest metallicity quarter from figure 3.14 was sub-divided in two (a_I and a_{II}) and four sections (a_1, a_2, a_3 and a_4) of equal number each.

Extremely low metallicity dependence







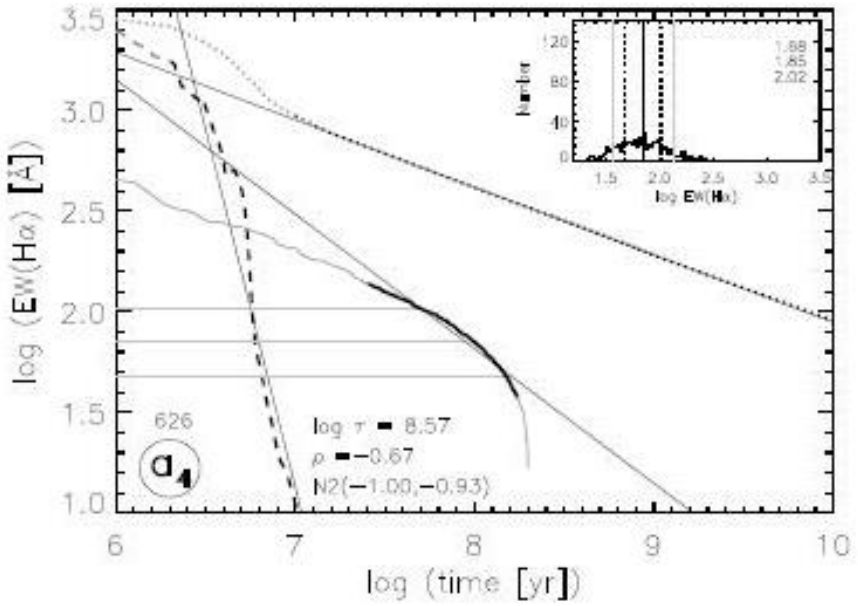


Figure 3.18: Inversion for data subsets of increasing metallicity. The letters correspond to the bins a_1, a_2, a_3 and a_4 in figure 3.16.

Metal content vs AGE

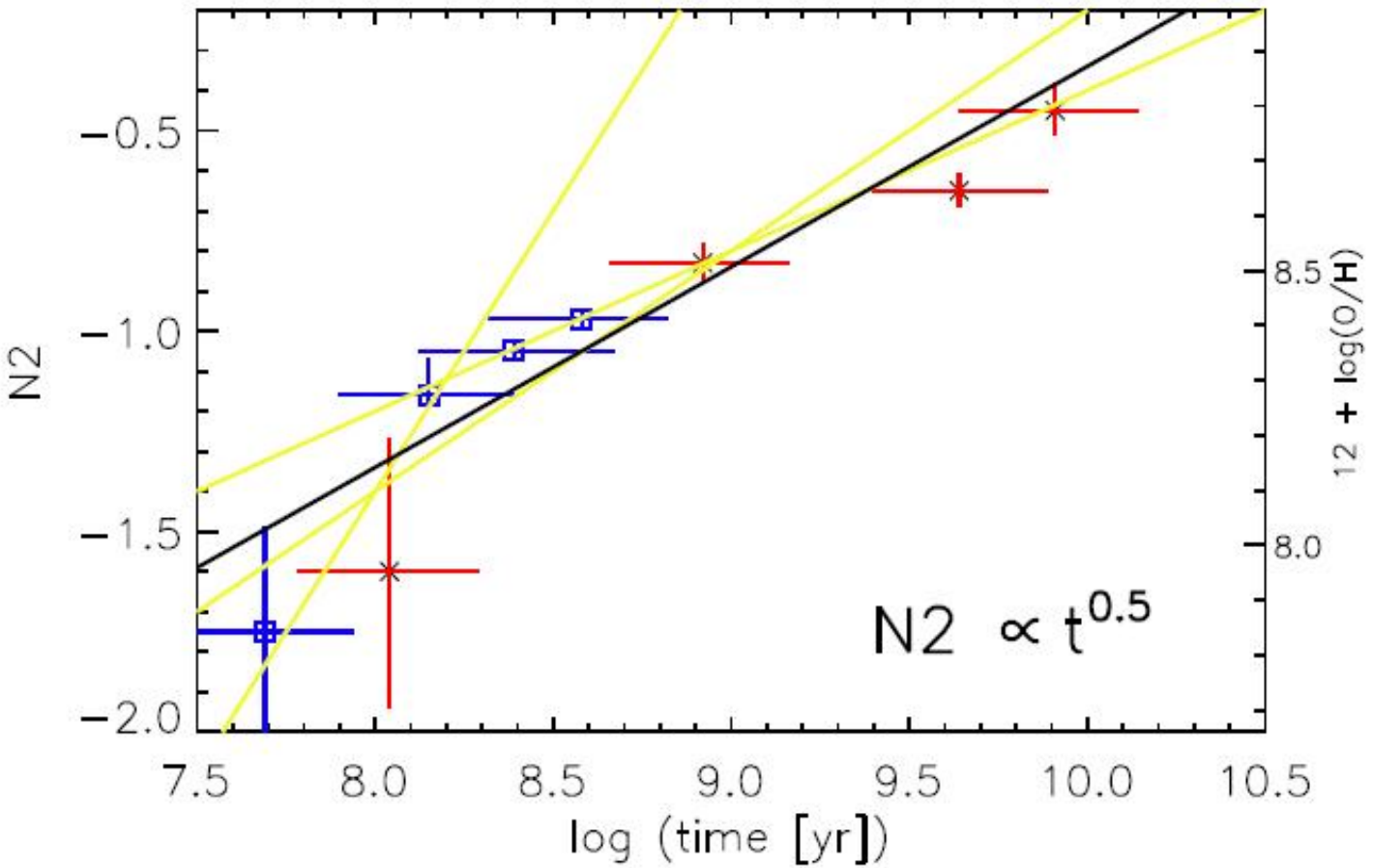


Figure 3.25: N2 and metallicity against time as obtained from different subsamples in figures 3.15 and 3.18. Bars are the range of values around the median (central 50% of the distribution).

Metal rich galaxies are older

Metallicity vs AGE for all HII galaxies

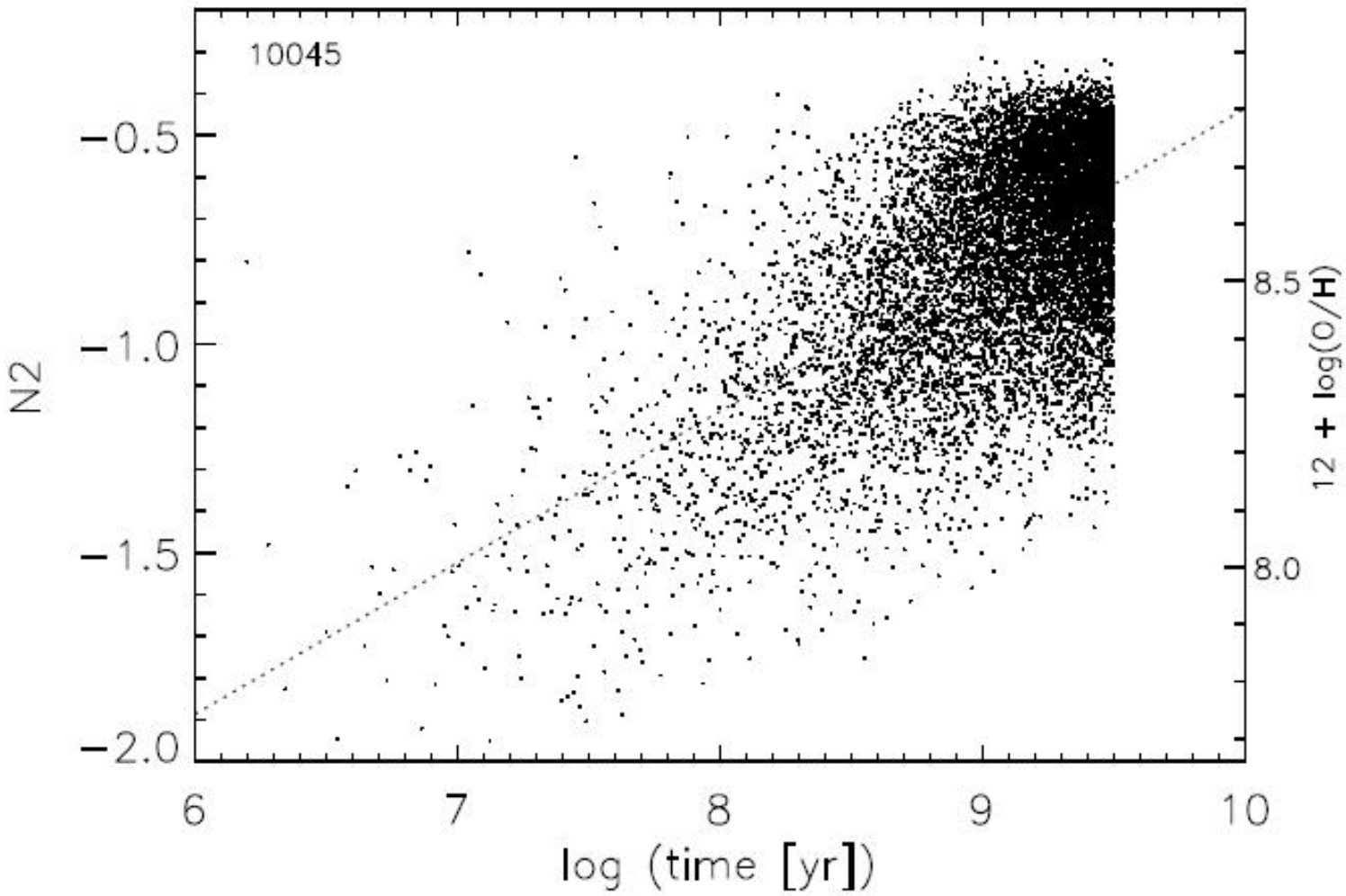


Figure 3.21: The metallicity indicator N2 as a function of time. The time is obtained from the whole sample inversion.

Distribution of IR luminosity (Z')

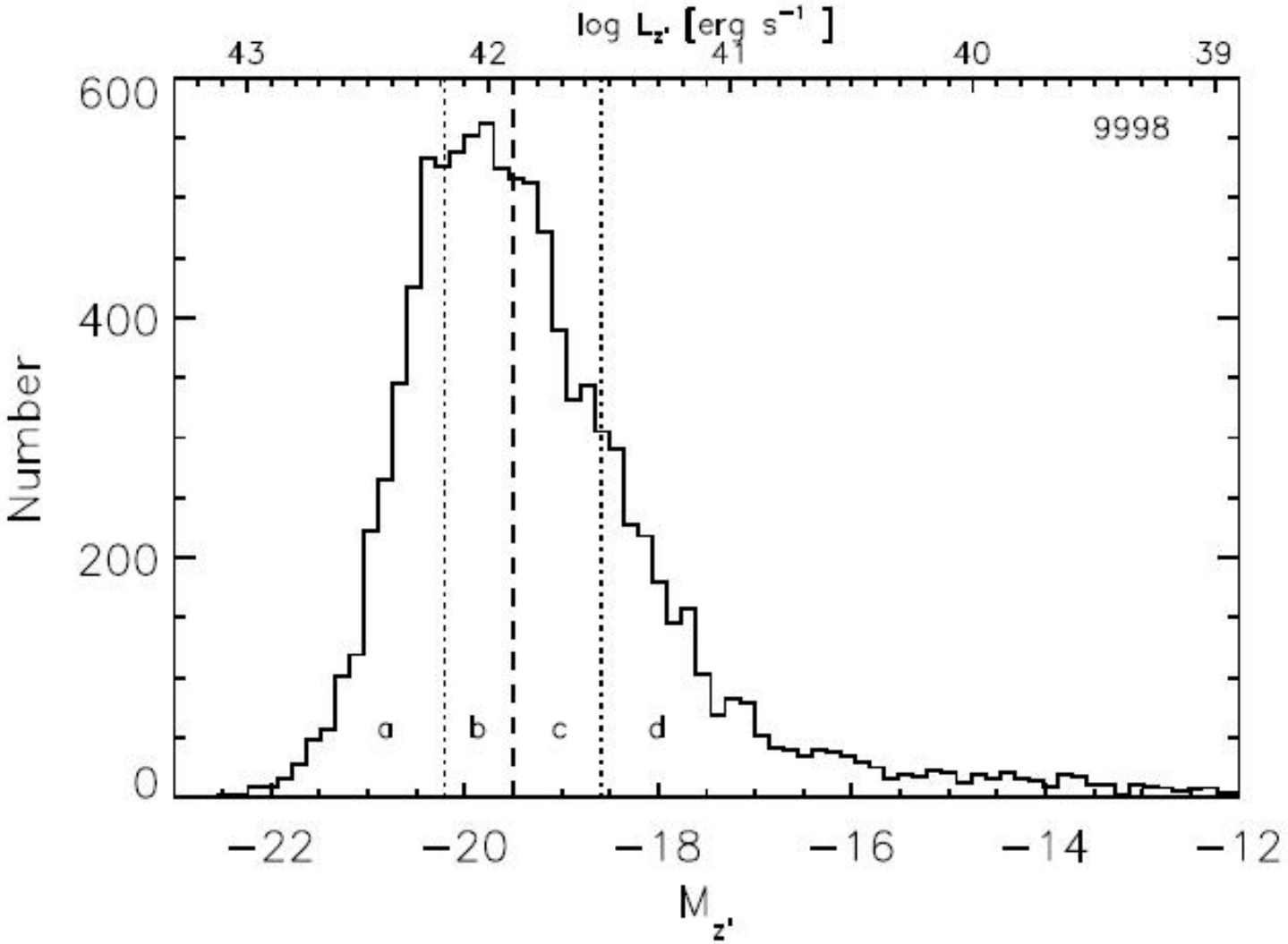


Figure 4.9: Distribution of absolute magnitude, the upper scale shows the luminosity

Mass estimate from IR luminosity and concentration parameter

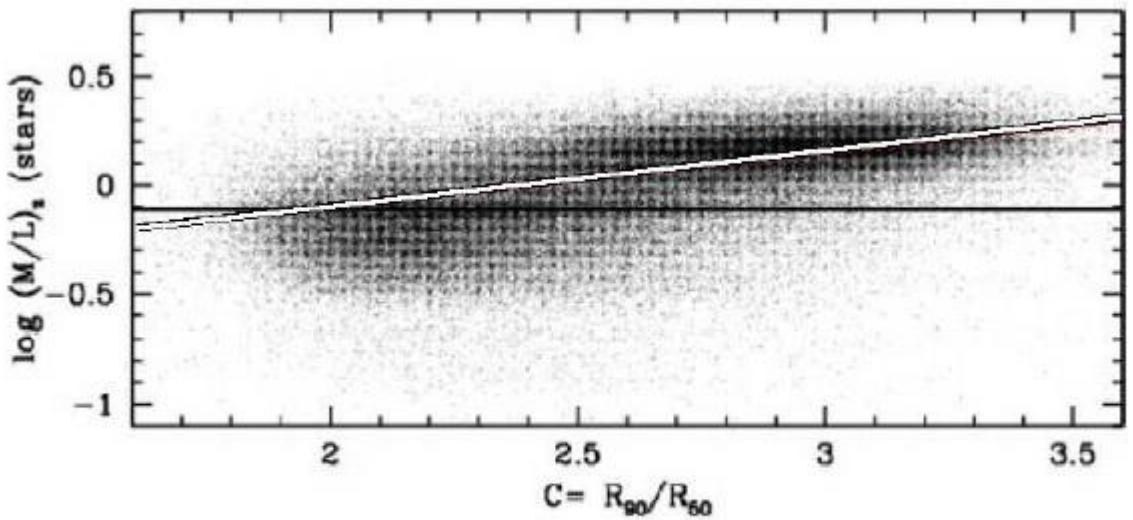


Figure 4.10: Log (M/L) in solar units as function of the concentration parameter (figure 13 from Kauffmann et al. (2003)). The line is the fit used to calculate the masses.

Mass distribution

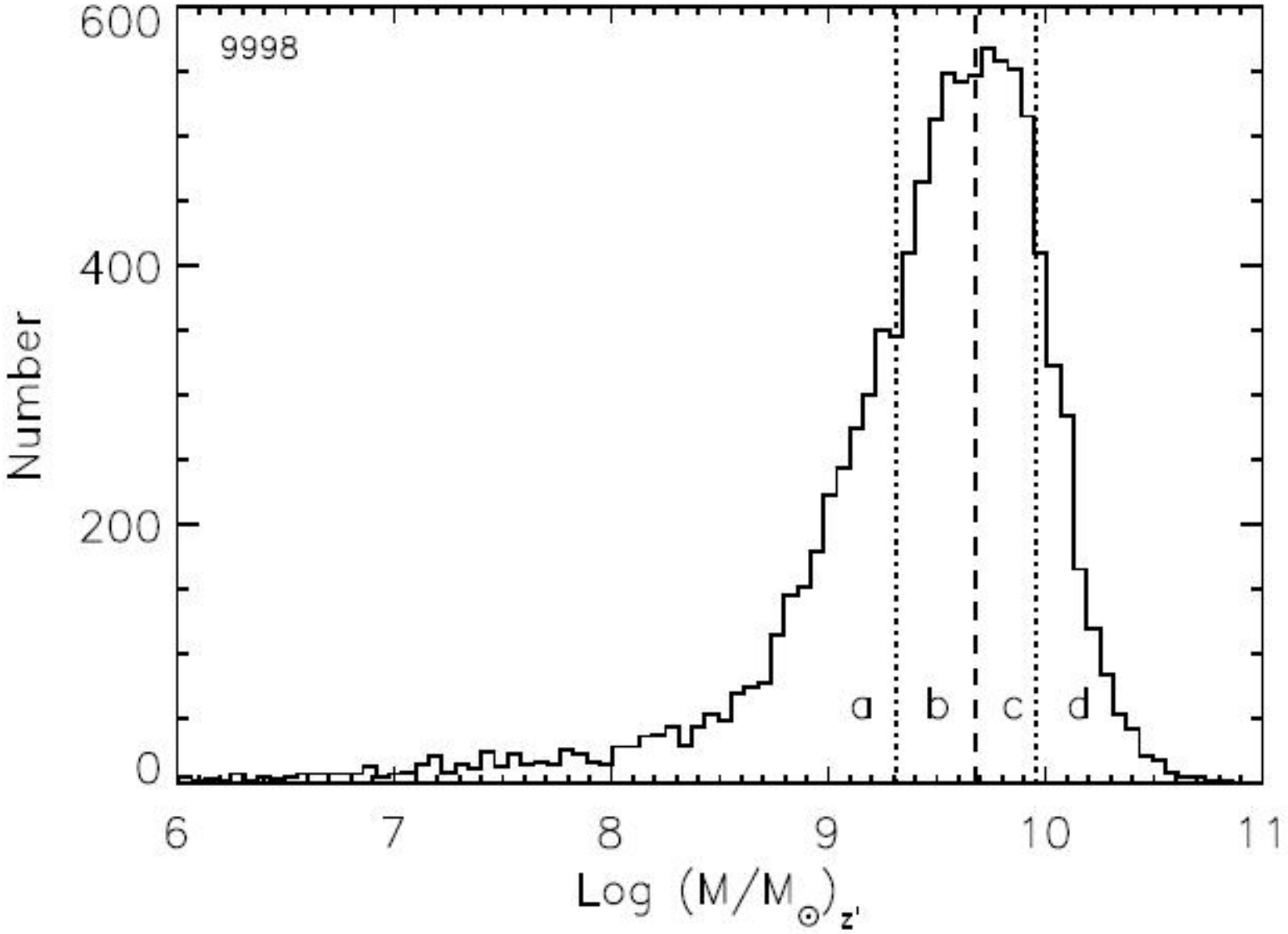


Figure 4.12: Mass distribution in solar units.

Mass dependence

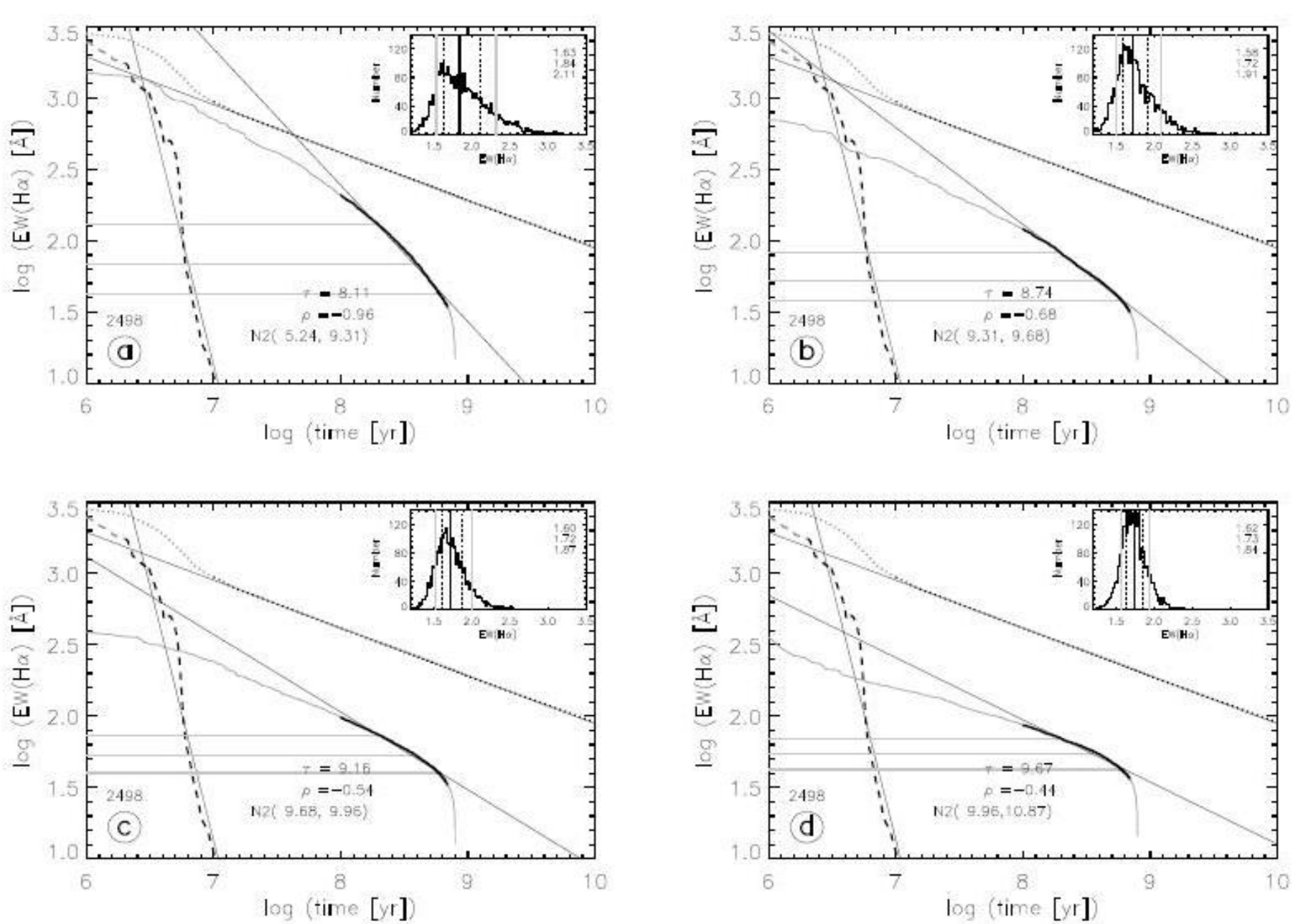


Figure 4.13: Inversion for data subsets of increasing mass. The letters correspond to the bins in figure 4.12.

Stellar mass vs AGE

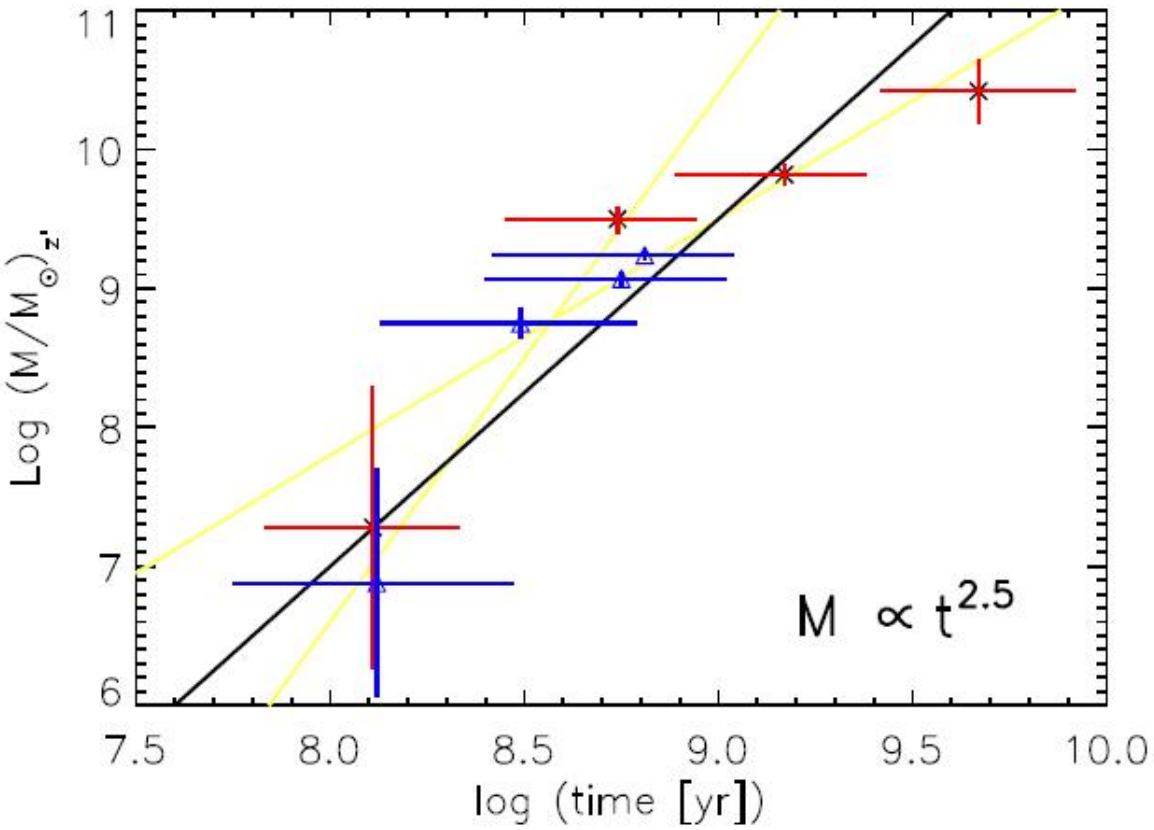


Figure 4.16: Mass as a function of time as obtained from the inversion over divisions in figure 4.12 (black symbols) and in figure 4.14 (grey symbols). The black line represents a time dependence on the mass of the form $\sim M \propto t^{2.5}$. Bars are the range of values around the median (centra 50 % of the distribution).

Massive galaxies are older.

Low mass galaxies are younger

Slope of the SFR vs AGE

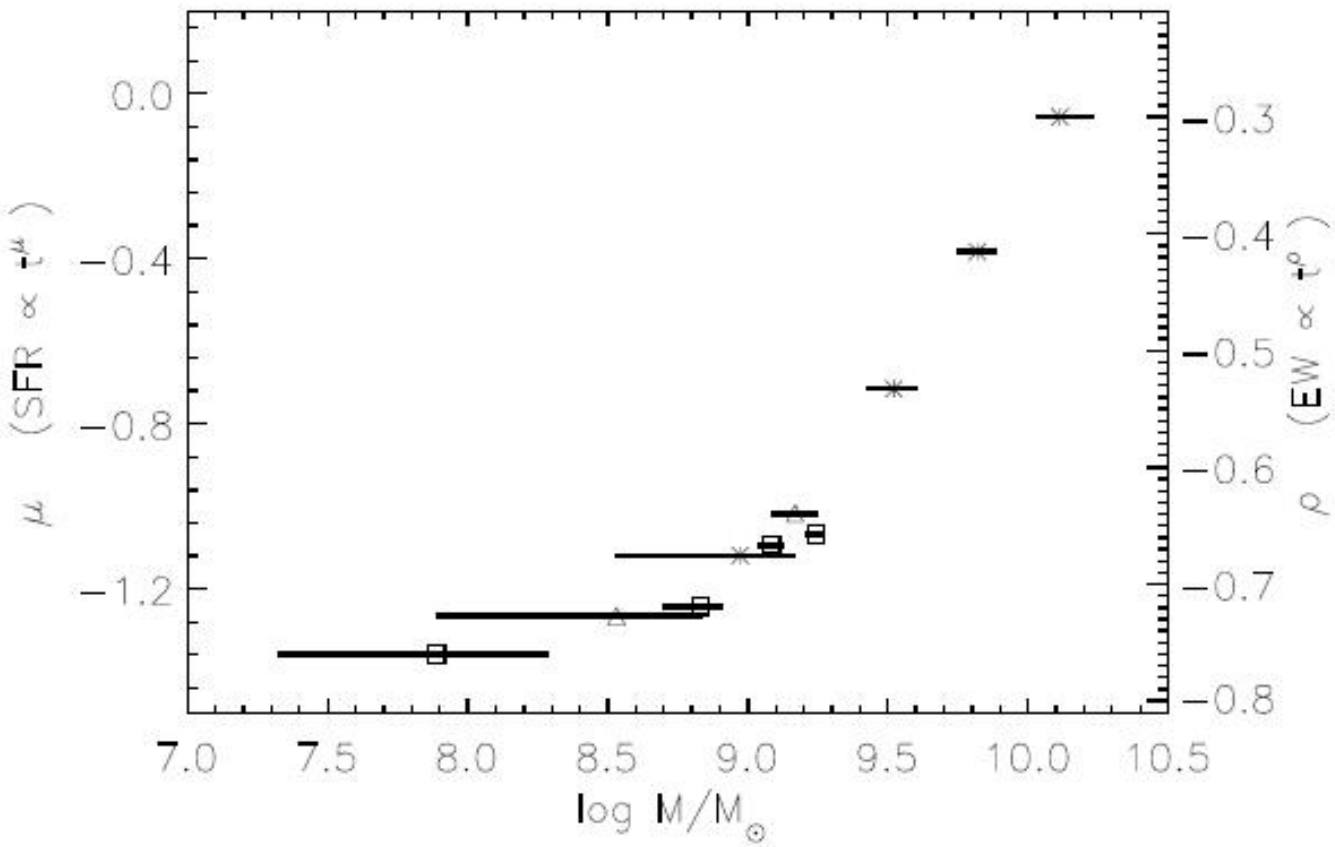


Figure 4.17: SFR (μ) and EW (ρ) power law indices as a functions of mass. Bins a, b, c and d from figure 4.12 correspond to asterisk symbols. Bins from figure 4.14 correspond to squares. The horizontal lines show the extent from the second to the third quarter (central 50 % of the distribution), the symbol indicates the median for each mass bin.

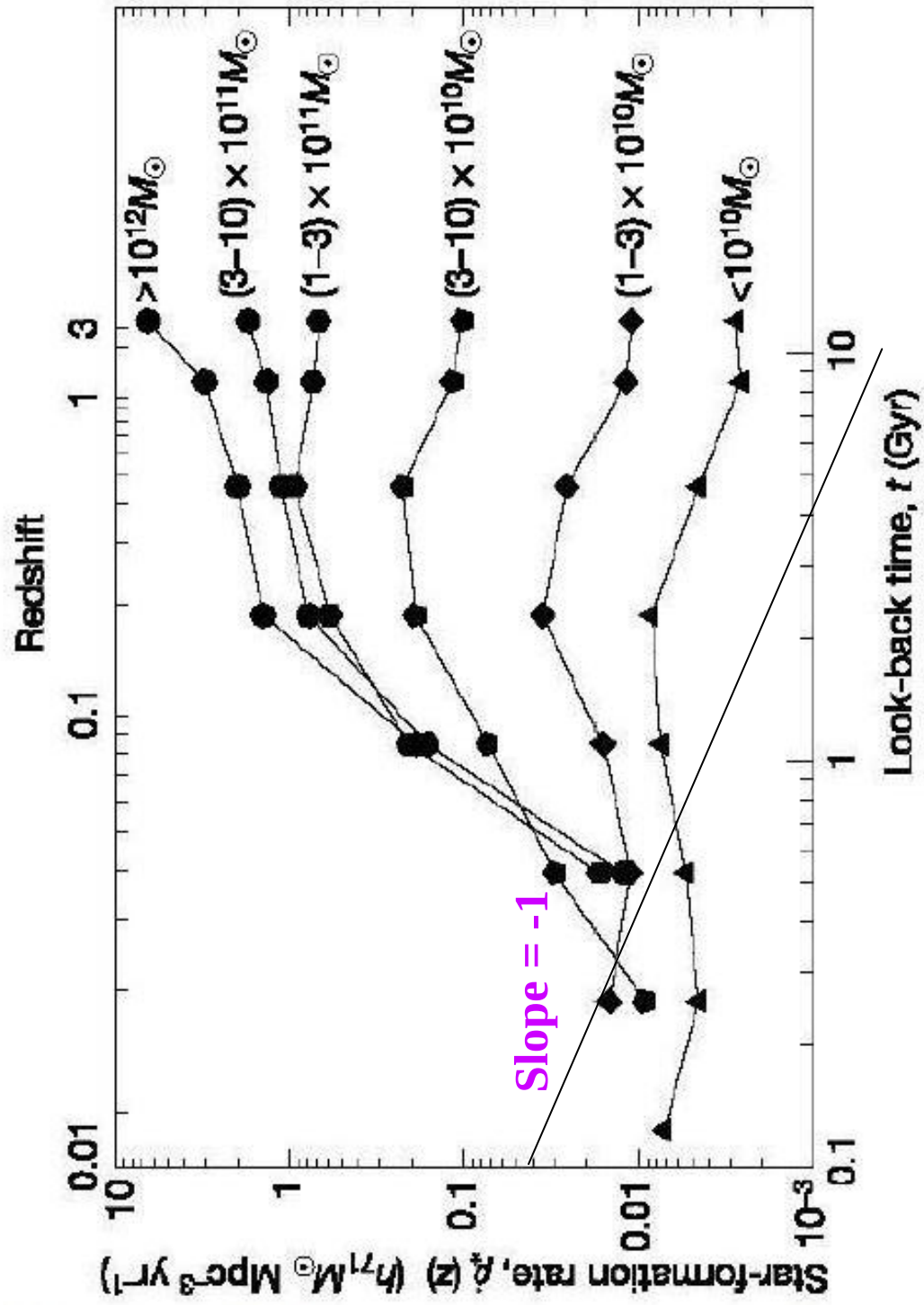


Figure 4.18: SFR vs. lookback time as a function of the galaxy mass (from (Heavens et al., 2004)).

Conclusions

The Madau diagram is an average over galaxy mass

Galaxy formation seems to follow different paths according to total mass.

Our analysis indicates that:

- Massive galaxies formed in a short time long time ago.
- Low mass galaxies are still forming
- Very low mass galaxies have not yet reach their maximumSFR.

All this supports downsizing even down to the lowest mass galaxies known

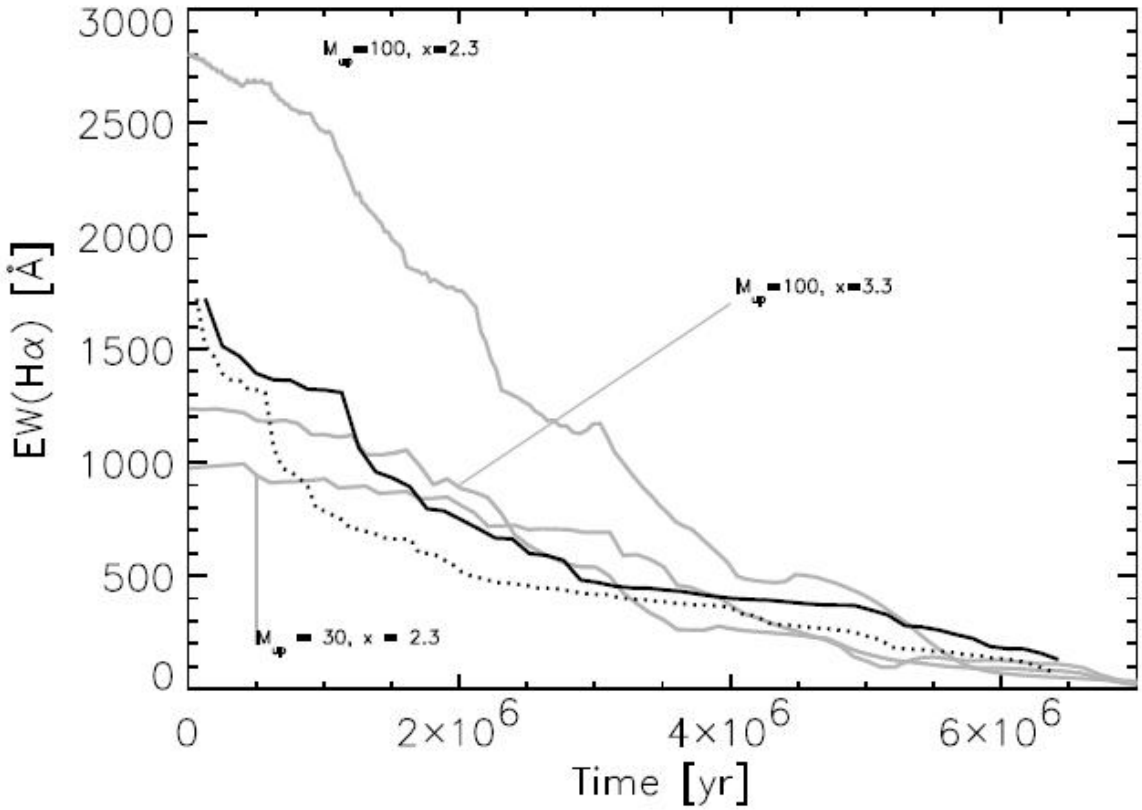


Figure 3.19: Restricted metallicity inversions compared with SB models (grey lines). Inversions are for the 50 (solid black line), and the 100 lowest metallicity objects (dotted black line).